Local buckling of stainless steel plates in fire

Zhe Xing[a], Merih Kucukler[b,*], Leroy Gardner[a]

[a]*Department of Civil and Environmental Engineering, Imperial College London, London, SW7 2AZ, UK*
[b]*School of Engineering, University of Warwick, Coventry, CV4 7AL, UK*

Abstract

The local buckling behaviour and design of stainless steel plates in fire are investigated in this paper. Finite element models of stainless steel plates able to mimic their response in fire are created and validated against experimental results from the literature. Parametric studies are then performed and the results are utilised to assess the current design provisions set out in the European structural steel fire design code EN 1993-1-2; shortcomings in the prediction of the local buckling response of stainless steel plates in fire are revealed. A new effective width based design approach able to reflect the variation in strength and stiffness of stainless steel at different temperature levels in the determination of the local plate slenderness and thereby the ultimate resistances of stainless steel plates in fire is put forward. The proposed approach is shown to provide significantly higher levels of accuracy and reliability relative to the current provisions in EN 1993-1-2 for a wide range of plate slendernesses, elevated temperature levels, stainless steel grades and loading conditions. Incorporation of the proposed design approach into future revisions of EN 1993-1-2 is recommended.

Keywords: Fire; Local buckling; Stainless steel; Finite element modelling; Plate buckling; Cross-section classification

1. Introduction

Stainless steel displays higher strength and stiffness retention at elevated temperatures in comparison to carbon steel, resulting in enhanced structural fire performance for stainless steel structures; this is increasingly being recognised by the construction and offshore industries [1, 2]. Stainless steel members with slender cross-sections are common; in these cross-sections, local instabilities prevent attainment of the full cross-section resistances and must be taken into account in both room temperature and elevated temperature design. However, despite the significantly varying material response of stainless steel at elevated temperatures, the European structural steel fire design code EN 1993-1-2 [3] merely directs the designer to the methods presented in EN 1993-1-4 [4] for the local buckling assessment of stainless steel plates in fire. The design methods in EN 1993-1-4 [4] were developed considering the room temperature local buckling response of

*Corresponding author

Email addresses: zhe.xing16@imperial.ac.uk (Zhe Xing), merih.kucukler@warwick.ac.uk (Merih Kucukler), leroy.gardner@imperial.ac.uk (Leroy Gardner)

stainless steel plates, thus typically failing to accurately represent the local buckling behaviour of stainless steel plates in fire.

Previous research into the local buckling response of stainless steel plates in fire is rather limited, though there have been a number of studies into member buckling [5–10]. Conversely, there has been a number of studies into the local buckling response of carbon steel plates at elevated temperatures [11–15]. Ranby [11] showed that while use of the elevated temperature strength at 2% total strain $f_{2,\theta}$ as the reference strength leads to accurate ultimate cross-section strength predictions for Class 1, 2 and 3 cross-sections owing to the attainment of high strains levels in structural elements in fire, adoption of the elevated temperature 0.2% proof strength $f_{\mathrm{p0.2},\theta}$ is generally more appropriate for Class 4 cross-sections since local buckling precludes the attainment of high strain levels. The recommendations of Ranby [11] were adopted in EN 1993-1-2 [3]. However, recently, Couto et al. [13] highlighted shortcomings of this approach, particularly at the transition between Class 3 and Class 4 cross-sections where a discontinuity in strength predictions exists due to the adoption of the different reference strengths (i.e. $f_{2,\theta}$ and $f_{\mathrm{p0.2},\theta}$). To eliminate this discontinuity, the use of the elevated temperature strength at 2% total strain $f_{2,\theta}$ for the ultimate cross-section strength predictions of all cross-sections regardless of their class was proposed in [13], in conjunction with a new set of effective width formulations for the local buckling assessment of carbon steel plates in fire. However, previous investigations have focused only on the response of carbon steel plates at elevated temperatures, and the local buckling behaviour of stainless steel elements in fire remains relatively unexplored.

With the aim of filling this gap in knowledge, the current paper investigates the local buckling response of stainless steel plates at elevated temperatures. Finite element models of stainless steel plates are first created to replicate their behaviour in fire, and then validated against a series of experimental results from the literature. Shortcomings of the existing design provisions in EN 1993-1-2 [3] for the local buckling assessment of stainless steel plates in fire are illustrated through comparisons with the results from the validated finite element models. A new effective width-based design method, utilising the strength at 2% total strain $f_{2,\theta}$ as the reference strength, is proposed to determine the local buckling strength of stainless steel plates at elevated temperatures. The accuracy and reliability of the proposed method are thoroughly verified against the results from the nonlinear finite element modelling, considering various elevated temperature levels, stainless steel grades and plate slendernesses.

2. Finite element modelling

The development and validation of finite element models able to replicate the response of stainless steel plates in fire are presented in this section. The finite element models are used in Section 3 for the assessment of the current EN 1993-1-2 design provisions and in Section 4 and 5 for the establishment and verification of the new proposals.

2.1. Development of finite element models

The finite element analysis software Abaqus [16] was used for all the numerical simulations carried out in the current study. Two categories of stainless steel plates were considered: (i) a 1600 mm $\times$ 400 mm plate with both longitudinal edges simply-supported, mimicking the response of

the internal elements of stainless steel cross-sections and (ii) a 4000 mm × 400 mm plate with one longitudinal edge simply-supported and the other longitudinal edge free, replicating the response of outstand flanges of open stainless steel sections. Note that the dimensions of the internal stainless steel plate elements were selected in accordance with those adopted by Couto et al. [13], while the dimensions of the outstand plate elements, which show no elastic buckling minimum and are more sensitive to length effects were modified in this paper to obtain elastic buckling stress values in closer agreement with analytical results for long plates [17–19]. Finite element models of both hot-rolled and cold-formed stainless steel plates were created. The four-noded reduced integration general purpose shell finite element S4R [16], which has been successfully adopted for similar previous applications [20–24], was used to create all the finite element models. The element size was taken as 20 mm by 20 mm (i.e. 20 elements across the 400 mm plate width) for all plates. This mesh size was chosen on the basis of a prior mesh sensitivity study. It should be noted that in this paper, grade 1.4301 austenitic, grade 1.4462 duplex and grade 1.4003 ferritic stainless steel were considered to generally represent the common grades of austenitic, duplex and ferritic stainless steel respectively. To represent the elevated temperature stress-strain (σ-ε) response of stainless steel, the two-stage compound Ramberg–Osgood material model [25–27] was utilised, as adopted by Kucukler et al. [28], and given by eqs. (1) and (2):

$$\varepsilon = \frac{\sigma}{E_\theta} + 0.002\left(\frac{\sigma}{f_{\mathrm{p0.2},\theta}}\right)^{n_\theta} \quad \text{for} \quad \sigma \leq f_{\mathrm{p0.2},\theta} \tag{1}$$

$$\varepsilon = \frac{\sigma - f_{\mathrm{p0.2},\theta}}{E_{\mathrm{p0.2},\theta}} + \left(\varepsilon_{\mathrm{u},\theta} - \varepsilon_{\mathrm{p0.2},\theta} - \frac{f_{\mathrm{u},\theta} - f_{\mathrm{p0.2},\theta}}{E_{\mathrm{p0.2},\theta}}\right)\left(\frac{\sigma - f_{\mathrm{p0.2},\theta}}{f_{\mathrm{u},\theta} - f_{\mathrm{p0.2},\theta}}\right)^{m_\theta} + \varepsilon_{\mathrm{p0.2},\theta} \quad \text{for} \quad f_{\mathrm{p0.2},\theta} < \sigma \leq f_{\mathrm{u},\theta}, \tag{2}$$

where n_θ and m_θ are strain hardening exponents, E_θ is the modulus of elasticity at temperature θ, and $E_{\mathrm{p0.2},\theta}$ and $\varepsilon_{\mathrm{p0.2},\theta}$ are the tangent modulus and total strain respectively corresponding to $f_{\mathrm{p0.2},\theta}$ and $f_{\mathrm{u},\theta}$ and $\epsilon_{\mathrm{u},\theta}$ are the ultimate tensile strength and strain at temperature θ. It was ensured that the second stage of the Ramberg-Osgood material model passed through $f_{2,\theta}$ and $f_{\mathrm{u},\theta}$ exactly at 2% total strain and the ultimate strain $\varepsilon_{\mathrm{u},\theta}$ respectively by adopting m_θ values calculated from:

$$m_\theta = \frac{\ln\left(\dfrac{0.02 - \varepsilon_{\mathrm{p0.2},\theta} - \dfrac{f_{2,\theta} - f_{\mathrm{p0.2},\theta}}{E_{\mathrm{p0.2},\theta}}}{\varepsilon_{\mathrm{u},\theta} - \varepsilon_{\mathrm{p0.2},\theta} - \dfrac{f_{\mathrm{u},\theta} - f_{\mathrm{p0.2},\theta}}{E_{\mathrm{p0.2},\theta}}}\right)}{\ln\left(\dfrac{f_{2,\theta} - f_{\mathrm{p0.2},\theta}}{f_{\mathrm{u},\theta} - f_{\mathrm{p0.2},\theta}}\right)} \tag{3}$$

as defined in [29] and illustrated in Fig. 1. The elevated temperature material properties (i.e. $f_{\mathrm{p0.2},\theta}$, $f_{2,\theta}$, $f_{\mathrm{u},\theta}$, $\varepsilon_{\mathrm{u},\theta}$ and E_θ) utilised in the Ramberg-Osgood material model given in eqs. (1) and (2) were determined by multiplying the standardised room temperature material properties set out in [30] by the corresponding strength ($k_{\mathrm{p0.2},\theta}$, $k_{2,\theta}$), stiffness ($k_{\mathrm{E},\theta}$) and ductility ($k_{\varepsilon_{\mathrm{u},\theta}}$) reduction factors

given in the SCI Structural Stainless Steel Design Manual [31], which are based on the results from extensive elevated temperature material testing [32–35], i.e. $f_{\mathrm{p0.2},\theta} = k_{\mathrm{p0.2},\theta} f_{\mathrm{y}}$, $f_{2,\theta} = k_{2,\theta} f_{\mathrm{y}}$, $E_\theta = k_{E,\theta} E$, $f_{\mathrm{u},\theta} = k_{\mathrm{u},\theta} f_{\mathrm{u}}$ and $\varepsilon_{\mathrm{u},\theta} = k_{\varepsilon_{\mathrm{u}},\theta} \varepsilon_{\mathrm{u}}$. The standardised room temperature material properties [30] of hot-rolled and cold-formed austenitic, duplex and ferritic stainless steel plates used to determine $f_{\mathrm{p0.2},\theta}$, $f_{2,\theta}$, $f_{\mathrm{u},\theta}$, $\varepsilon_{\mathrm{u},\theta}$ and E_θ are given in Table 1, where f_y is the 0.2% proof stress, f_{u} is the ultimate tensile strength, ε_u is the ultimate tensile strain and n is the Ramberg-Osgood exponent used to define the first stage of the stress-strain response. In accordance with the recommendations made in [31], the elevated temperature Ramberg Osgood exponents n_θ used in eqs. (1) and (2) were taken equal to the room temperature values n given by [30], which are shown in Table 1.

The boundary conditions applied to the finite element models of the internal and outstand stainless steel plates are illustrated in Fig. 2. As can be seen from the figure, to simulate simply-supported restraint conditions along the longitudinal edges, only the vertical translations were restrained (i.e. $U3 = 0$). For the loaded edges, the vertical translations were also restrained (i.e. $U3 = 0$) in addition to the horizontal translations (i.e. $U2 = 0$) at the mid-width nodes. Finally, the mid-width node of one of the loaded edges were restrained along the longitudinal direction ($U1 = 0$). Loading was applied as point forces and/or bending moments to reference points constrained to the loaded edges as shown in Fig. 2. Elastic buckling stresses obtained from the Linear Buckling Analyses (LBA) of the developed finite element plate models were compared against elastic buckling stresses calculated using the formulae provided in [17, 36]; excellent agreement was observed between the numerically and analytically determined elastic buckling stress values, verifying the appropriateness of the boundary and loading conditions applied to the finite element models.

The lowest eigenmode-affine imperfection shapes obtained from Linear Buckling Analyses (LBA) of the modelled plates, as shown in Fig. 3, were used to define the shapes of local geometrical imperfections in the finite element simulations; these imperfection shapes were scaled to 1/200 of the plate widths for the internal elements and 1/50 of the plate widths for the outstand flanges in accordance with the recommendations made in EN 1993-1-5 [37]. Considering their negligible effect on the ultimate resistances of steel plates at elevated temperatures, as shown in [13], residual stresses were not explicitly taken into account in the finite element models created herein, though their influence does inherently feature in the stress-strain properties of the cold-formed material [38]. Typical failure modes from the finite element models of the internal and outstand stainless steel plates under compression are illustrated in Fig. 4.

2.2. Validation of numerical models

In this subsection, the adopted finite element modelling approach has been validated through comparisons of the FE results with the results obtained from fire experiments carried out on stainless steel hollow section stub columns by Uppfeldt et al. [39] and on stainless steel beams by Gardner and Baddoo [40].

2.2.1. Uppfelt et al. [39] tests

The finite element modelling approach adopted in this study for stainless steel plates in compression was validated using the experimental results of Uppfeldt et al. [39], where six stainless

steel square hollow section (SHS) stub columns were tested in fire. On the basis of the stub column failure loads reported in [39], the experimental failure loads of the plates constituting the stub columns were calculated considering their corresponding areas and compared against the numerical failure loads of the plates. In the finite element models of the plates, the plate sizes were determined considering the flat parts and corner regions of the stub columns of [39] as shown in Fig. 5, taking the thicknesses of the plates equal to the thicknesses of the stub columns t and the widths of the plates equal to the centreline widths of the stub column cross-sections ($h-t$). Twenty elements were defined across the width of the modelled stainless steel plates and an element aspect ratio of unity (i.e. square elements) was maintained throughout. The two-stage compound Ramberg-Osgood material model given by eqs. (1) and (2) was used to define the material response of the specimens in fire, using the elevated temperature material properties determined by multiplying the strength and stiffness reduction factors given in [31] by the corresponding room temperature material properties of the specimens obtained from a series of tensile coupon tests reported by Uppfeldt et al. [39]. The enhanced strengths of the corner regions owing to cold-working were allowed for in the material properties of the plates by using the following expression to determine their weighted-average room temperature 0.2% proof strengths:

$$f_{\mathrm{y}} = \frac{f_{\mathrm{y,flat}} A_{\mathrm{flat}} + f_{\mathrm{y,corner}} A_{\mathrm{corner}}}{A_{\mathrm{flat}} + A_{\mathrm{corner}}}, \tag{4}$$

where $f_{\mathrm{y,flat}}$ and $f_{\mathrm{y,corner}}$ are the 0.2% proof strengths of the flat and corner regions and A_{flat} and A_{corner} are the areas of the flat and corner regions, respectively. The local geometric imperfection amplitudes in the finite element models were taken as the measured values reported in [39]. Table 2 summarizes the failure loads of the plates determined from the tests $N_{\mathrm{u,test}}$ and those obtained from the finite element models $N_{\mathrm{u,FE}}$. As can be seen from the table, the $N_{\mathrm{u,FE}}$/ $N_{\mathrm{u,test}}$ values are generally close to unity with reasonable scatter, indicating that the finite element models are able to provide accurate estimations of the ultimate resistances of compressed stainless steel internal plate elements in fire.

2.2.2. Gardner and Baddoo [40] tests

The finite element modelling approach adopted in this study for stainless steel internal plate elements in bending and outstand flanges in compression was validated using the results from three anisothermal tests performed on stainless steel beams at elevated temperatures reported in [40], where one stainless steel rectangular hollow section (RHS) beam and two stainless steel I-section beams were tested in fire. Since the determination of the failure forces and moments of the isolated web and flange plates of the beams is not straightforward owing to the varying level of support afforded by the flange plates to the web plates and vice versa, the full beam cross-sections were modelled instead of the individual plates. The FE failure moments $M_{\mathrm{u,FE}}$ were then compared against those obtained from the experiments $M_{\mathrm{u,test}}$. Note that for the SHS stub columns considered in the previous section, all four internal plate elements have the same elastic local buckling stress and half-wavelength; the plates therefore buckle simultanously and mirror the response of isolated plates with simply-supported boundary conditions along the adjoined edges [18, 19]. In the full beam finite element models created herein, the element type and mesh size (i.e. 20 elements across the width of each plate and an element aspect ratio of unity) were taken to be the same

as those employed in the finite element models of the individual plates. The measured material properties were taken as those measured in the corresponding experiments, while the geometric imperfections, which were not measured in the testing programme, were modelled as described in Section 2.1. The test and FE results are compared in Table 3, where it can be seen that there is close agreement between the two. Thus, further to the validation for stainless steel internal plate elements in compression presented in Section 2.2.1, the adopted finite element modelling approach is also considered to be appropriate for the simulation of stainless steel internal plate elements in bending and outstand flange elements in compression.

2.3. Parametric study

Upon validation of the numerical models, parametric studies were conducted to generate comprehensive structural performance data, taking into consideration different stainless steel grades (austenitic, duplex and ferritic), elevated temperature levels, plate thicknesses and loading conditions. In total, four temperature levels were considered: 200 °C, 400 °C, 600 °C and 800 °C. The plate thicknesses were varied to investigate the response of stainless steel plates with a spectrum of local elevated temperature plate slendernesses $\bar{\lambda}_{\mathrm{p},\theta}$ (see Section 4.2) ranging between 0.15 and 2.0. Thus, plate thicknesses ranging between about 2 mm and 80 mm were considered in the numerical parametric studies of the internal elements, while the thicknesses of the outstand elements were varied between about 12 mm and 200 mm. Note that, since relatively wide plates were considered (particularly for the outstand flanges), rather large plate thicknesses were needed to achieve low plate slenderness values. Stainless steel plates under compression, bending and combined compression and bending were considered. Combined compression and bending was applied such that the ratios ψ of the stresses applied at the edges of the plates (σ_1 and σ_2) were equal to 0.5, 0 and -0.5 (i.e. $\psi = \sigma_1/\sigma_2 = 0.5, 0, -0.5$).

3. Current EN 1993-1-2 design method for stainless steel in fire

The EN 1993-1-2 [3] cross-section classification and effective width-based design rules for determining the local buckling strengths of stainless steel plates in fire are briefly described in this section; their accuracy is then assessed against the results obtained from nonlinear finite element modelling.

3.1. Cross-section classification

For the classification of stainless steel cross-sections in fire, EN 1993-1-2 [3] directs the designer to EN 1993-1-4 [4] but with a reduced value for material factor ε_θ, where stainless steel cross-sections are grouped into four classes; the class of a cross-section is taken as the highest class of its constituent plates. Specific limiting width-to-thickness ratios, summarised in Table 4, are given for the constituent internal and outstand plates of stainless steel sections in EN 1993-1-4 [4] to determine their classes. At elevated temperatures, the material factor ε_θ is calculated as:

$$\varepsilon_\theta = 0.85\varepsilon = 0.85\left[\frac{235}{f_{\mathrm{y}}}\frac{E}{210000}\right]^{0.5} \quad \text{with } f_{\mathrm{y}} \text{ and } E \text{ in MPa,} \tag{5}$$

where ε is the room temperature material factor given in EN 1993-1-4 [4]; note that the definition of ε is due to be simplified to $\varepsilon = (235/f_y)^{0.5}$ in the upcoming version of the code. While this classification approach leads to the straightforward determination of the class of a stainless steel cross-section in fire, it disregards the differential erosion of the strength and stiffness of stainless steel at different temperature levels, which is shown in Fig. 6. In fact, the 0.85 factor was originally derived considering the lowest value of the square root of the ratios of the stiffness reduction factors to the yield strength reduction factors $\sqrt{k_{E,\theta}/k_{2,\theta}}$ for carbon steel and is somewhat inappropriate for stainless steel, as shown in Fig. 6. Thus, despite its practicality, the cross-section classification approach provided in EN 1993-1-2 [3] does not provide a sound basis for assessing the response of stainless steel cross-sections at elevated temperatures.

3.2. Effective width method

Thin plates subjected to in-plane compressive loading exhibit a stable post-buckling response, enabling load-carrying capacities beyond the critical buckling load to be sustained. After buckling occurs, the stress distribution across the plate width becomes non-uniform. In the effective width method, this non-uniform stress distribution is simplified into two uniform stress blocks with a width of $b_{\text{eff}}/2$ as shown in Fig. 7 and the effective widths of stainless steel plates are calculated using the following expression [41]:

$$b_{\text{eff}} = \rho b, \tag{6}$$

where ρ is the plate buckling reduction factor. EN 1993-1-2 [3] also directs the designer to EN 1993-1-4 [4] for the determination of the plate buckling reduction factor ρ based on room temperature material properties. For internal elements, ρ is calculated as [3, 4]:

$$\rho = \frac{0.772}{\bar{\lambda}_{\text{p}}} - \frac{0.079}{\bar{\lambda}_{\text{p}}^2} \quad \text{but} \quad \rho \leq 1.0, \tag{7}$$

while for the outstand flanges, ρ is determined from [3, 4]:

$$\rho = \frac{1}{\bar{\lambda}_{\text{p}}} - \frac{0.188}{\bar{\lambda}_{\text{p}}^2} \quad \text{but} \quad \rho \leq 1.0, \tag{8}$$

in which $\bar{\lambda}_{\text{p}}$ is the non-dimensional plate slenderness, calculated as:

$$\bar{\lambda}_{\text{p}} = \sqrt{\frac{f_y}{\sigma_{\text{cr}}}} = \frac{b/t}{28.4\varepsilon\sqrt{k_\sigma}}, \tag{9}$$

where σ_{cr} is the elastic buckling stress of the plate, t is the plate thickness and k_σ is the buckling coefficient determined on the basis of the stress distribution and edge boundary conditions of the plate as described in [37]. Note that an alternative approach to treating local buckling on an element by element basis is to consider the elastic buckling stress of the full cross-section, as described in [18].

It is worth noting that while EN 1993-1-2 [3] requires the use of the elevated temperature material factor $\epsilon_\theta = 0.85\epsilon$ for the classification of stainless steel cross-sections in fire, it recommends the use of room temperature material properties for the determination of the effective cross-section

areas and effective section moduli of Class 4 stainless steel cross-sections at elevated temperatures. This represents an inconsistency in the consideration of the structural response of stainless steel cross-sections in fire in that even though the influence of changes in the material properties at elevated temperatures on the cross-section response is considered in the cross-section classification (albeit somewhat inappropriately), it is disregarded in the calculations of effective section properties used to determine the ultimate resistances of Class 4 stainless steel cross-sections in fire.

3.3. Cross-section resistance

The cross-section resistance of stainless steel structural elements in fire is defined in EN 1993-1-2 [3] on the basis of the classification of the section, as summarised in Table 5, where $N_{\mathrm{fi,t,Rd}}$ and $M_{\mathrm{fi,t,Rd}}$ are the axial and bending design cross-section resistances in fire at time t, respectively, A and A_{eff} are the gross and effective cross-sectional areas, W_{pl} is the plastic section modulus, W_{el} is the elastic section modulus, W_{eff} is the effective section modulus and $\gamma_{M,\mathrm{fi}}$ is the partial factor for fire design. The calculation of cross-sectional resistances of stainless steel structural elements in fire can be seen to be similar to their determination at room temperature except for the use of the elevated temperature strength at 2% strain $f_{2,\theta}$ for Class 1, 2 and 3 sections and the elevated temperature 0.2% proof strength $f_{\mathrm{p0.2},\theta}$ for Class 4 sections.

3.4. Assessment of EN 1993-1-2 provisions for the design of stainless steel plates in fire

The accuracy of the EN 1993-1-2 [3] provisions for the design of stainless steel internal and outstand plates in fire is assessed in this subsection against results from nonlinear shell finite element modelling considering different elevated temperature levels and room temperature non-dimensional plate slendernesses $\overline{\lambda}_{\mathrm{p}}$. Assessment of the EN 1993-1-2 [3] compression and bending resistance functions are shown in Fig. 8 and Fig. 9 for the case of hot-rolled stainless steel plates in fire. Further comparisons are shown in Section 5. As can be seen from the figures, EN 1993-1-2 [3] provides a single plate buckling curve to predict the ultimate axial compression and bending moment resistances of stainless steel plates at different elevated temperature levels; the ordinates of the plateaus of the plate buckling curves vary due to the different ratios of $f_{2,\theta}$ to $f_{\mathrm{p0.2},\theta}$ (i.e. $f_{2,\theta}/f_{\mathrm{p0.2},\theta}$) at different temperature levels and the use of the plastic and elastic section moduli to determine the bending moment resistances of stainless steel plates falling into the Class 1 and 2 and Class 3 categories, respectively. Since EN 1993-1-2 [3] utilises the elevated temperature strength at 2% strain $f_{2,\theta}$ for Class 1, 2 and 3 sections and the elevated temperature 0.2% proof strength for Class 4 sections, there is an abrupt step in local capacity at the plateau slenderness $\overline{\lambda}_{\mathrm{p,0}}$, which corresponds to the transition between Class 3 and Class 4 sections according to the classification limits provided in Table 4. Fig. 8 shows that the plate buckling curve of EN 1993-1-2 [3] yields inaccurate and rather conservative ultimate strength predictions for slender stainless steel plates under axial compression at high temperatures, particularly for the duplex and ferritic stainless steel grades. Moreover, the plateau lengths of the plate buckling curves $\overline{\lambda}_{\mathrm{p,0}}$ determined on the basis of the Class 3 classification limits given in Table 4 lead to significant overpredictions of the ultimate strengths of moderately slender austenitic stainless steel plates subjected to axial compression, indicating that shorter plateau lengths $\overline{\lambda}_{\mathrm{p,0}}$ are necessary.

4. New cross-section classification rules and effective width equations for stainless steel elements in fire

To enable accurate and safe ultimate strength predictions for stainless steel plates at elevated temperatures, new cross-section classification rules and effective width equations are presented in this section. In line with the effective width approach put forward in [13] for carbon steel plates in fire, the elevated temperature material strength at 2% strain $f_{2,\theta}$ is adopted as the sole reference strength for the determination of the ultimate strengths of stainless steel plates at elevated temperatures. A new system of cross-section classification is introduced whereby the four classes defined at room temperature are replaced with two classes – (i) non-slender and (ii) slender – at elevated temperature on the basis of whether or not $f_{2,\theta}$ can be reached. This simplifies design and is justified considering (i) a distinction between Class 1 and Class 2 sections, used to assess the applicability of the plastic design at room temperature, is not necessary in the fire design of steel structures and (ii) a much lower number cross-sections with practical proportions fall into the traditional Class 1, 2 and 3 categories than at room temperature owing to the use of the elevated temperature strength at 2% total strain $f_{2,\theta} = k_{2,\theta} f_y$. Note that, despite the differences in the adopted standardised material properties used to reflect hot-rolled and cold-formed stainless steel plates (see Table 1 [30]), the resulting structural behaviour was sufficiently similar that it was deemed that no distinction between the two is necessary for design purposes. This is in line with the current plate buckling design treatment for both carbon steel and stainless steel in Eurocode 3. In Section 5, the accuracy and reliability of the proposed effective method are verified and compared against the existing plate buckling assessment provisions set out in EN 1993-1-2 [3], taking into account various elevated temperature levels, stainless steel grades and plate slendernesses.

4.1. Classification of stainless steel cross-sections in fire

A new classification approach for stainless steel cross-sections in fire is introduced in this subsection. In the new cross-section classification approach, the class of a cross-section is determined on the basis of the classes of its constituent plates. A cross-section is classified as 'non-slender' only if all of its constituent plates are classified as 'non-slender'. When one or more plates constituting a cross-section are classified as 'slender', the cross-section is classified as 'slender'. For the classification of the individual stainless steel plates constituting a cross-section, the plateau slendernesses $\bar{\lambda}_{\mathrm{p0},\theta}$ given in eq. (11) and eq. (15) are used for austenitic stainless steel internal and outstand plates, while the plateu slendernesses $\bar{\lambda}_{\mathrm{p0},\theta}$ provided in eq. (13) and eq. (17) apply for duplex and ferritic stainless steel internal and outstand plates, respectively. If the elevated temperature slenderness $\bar{\lambda}_{\mathrm{p},\theta}$ of a plate determined using eq. (18) is less than the corresponding plateau slenderness $\bar{\lambda}_{\mathrm{p0},\theta}$, the plate is classified as 'non-slender', while if the plate slenderness $\bar{\lambda}_{\mathrm{p},\theta}$ is greater than the plateau slenderness $\bar{\lambda}_{\mathrm{p0},\theta}$, the plate is classified as 'slender'.

4.2. New effective width method for stainless steel plates in fire

To retain consistency between the room temperature and fire design of stainless steel cross-sections, the new effective width formulae proposed in this study follow a similar format to the existing effective width formulae in EN 1993-1-4 [4], but using the elevated temperature plate slenderness $\bar{\lambda}_{\mathrm{p},\theta}$ in lieu of room temperature plate buckling slenderness $\overline{\lambda}_{\mathrm{p}}$ to reflect the different

variations in strength and stiffness of stainless steel at elevated temperatures. The use of elevated temperature slenderness for local buckling is also consistent with the approach for member buckling.

For internal compression elements, the proposed reduction factors for the local buckling ρ of austenitic stainless steel plates are as follows:

$$\begin{aligned} \rho &= 1 \qquad\qquad \text{for} \quad \bar{\lambda}_{\mathrm{p},\theta} \leq \bar{\lambda}_{\mathrm{p0},\theta}, \\ \rho &= \frac{0.54}{\left(\bar{\lambda}_{\mathrm{p},\theta} / \sqrt{\xi_\theta}\right)^{0.75}} - \frac{0.015\,(3+\psi)}{\left(\bar{\lambda}_{\mathrm{p},\theta} / \sqrt{\xi_\theta}\right)^{1.5}} \quad \text{for} \quad \bar{\lambda}_{\mathrm{p},\theta} > \bar{\lambda}_{\mathrm{p0},\theta} \end{aligned} \tag{10}$$

with

$$\bar{\lambda}_{\mathrm{p0},\theta} = \left(0.27 + \sqrt{0.0279 - 0.015\psi}\right)^{1.33} \sqrt{\xi_\theta}. \tag{11}$$

For duplex and ferritic stainless steel internal plates, the proposed local buckling reduction factors ρ are:

$$\begin{aligned} \rho &= 1 \qquad\qquad \text{for} \quad \bar{\lambda}_{\mathrm{p},\theta} \leq \bar{\lambda}_{\mathrm{p0},\theta}, \\ \rho &= \frac{0.6}{\left(\bar{\lambda}_{\mathrm{p},\theta} / \sqrt{\xi_\theta}\right)^{0.75}} - \frac{0.015\,(3+\psi)}{\left(\bar{\lambda}_{\mathrm{p},\theta} / \sqrt{\xi_\theta}\right)^{1.5}} \quad \text{for} \quad \bar{\lambda}_{\mathrm{p},\theta} > \bar{\lambda}_{\mathrm{p0},\theta} \end{aligned} \tag{12}$$

with

$$\bar{\lambda}_{\mathrm{p0},\theta} = \left(0.3 + \sqrt{0.045 - 0.015\psi}\right)^{1.33} \sqrt{\xi_\theta}. \tag{13}$$

For outstand flanges, the proposed plate buckling reduction factors ρ for austenitic stainless steel are:

$$\begin{aligned} \rho &= 1 \qquad\qquad \text{for} \quad \bar{\lambda}_{\mathrm{p},\theta} \leq \bar{\lambda}_{\mathrm{p0},\theta}, \\ \rho &= \frac{0.6}{\left(\bar{\lambda}_{\mathrm{p},\theta} / \sqrt{\xi_\theta}\right)^{0.6}} - \frac{0.075}{\left(\bar{\lambda}_{\mathrm{p},\theta} / \sqrt{\xi_\theta}\right)^{1.2}} \quad \text{for} \quad \bar{\lambda}_{\mathrm{p},\theta} > \bar{\lambda}_{\mathrm{p0},\theta} \end{aligned} \tag{14}$$

with

$$\bar{\lambda}_{\mathrm{p0},\theta} = 0.237 \sqrt{\xi_\theta}. \tag{15}$$

For duplex and ferritic stainless steel outstand plates, it is proposed that ρ is calculated as follows:

$$\begin{aligned} \rho &= 1 \qquad\qquad \text{for} \quad \bar{\lambda}_{\mathrm{p},\theta} \leq \bar{\lambda}_{\mathrm{p0},\theta}, \\ \rho &= \frac{0.67}{\left(\bar{\lambda}_{\mathrm{p},\theta} / \sqrt{\xi_\theta}\right)^{0.6}} - \frac{0.075}{\left(\bar{\lambda}_{\mathrm{p},\theta} / \sqrt{\xi_\theta}\right)^{1.2}} \quad \text{for} \quad \bar{\lambda}_{\mathrm{p},\theta} > \bar{\lambda}_{\mathrm{p0},\theta} \end{aligned} \tag{16}$$

with

$$\bar{\lambda}_{\mathrm{p0},\theta} = 0.344 \sqrt{\xi_\theta}. \tag{17}$$

In eqs. (10), (12), (14) and (16), ψ is the ratio between the stresses at the edges of the plate as described in EN 1993-1-5 [37], $\overline{\lambda}_{\mathrm{p0},\theta}$ is the threshold plate slenderness below which $\rho = 1.0$ and $\bar{\lambda}_{\mathrm{p},\theta}$ is the elevated temperature plate slenderness calculated as:

$$\bar{\lambda}_{\mathrm{p},\theta} = \xi_\theta \sqrt{\frac{f_{\mathrm{y}}}{\sigma_{\mathrm{cr}}}} \quad \text{with} \quad \xi_\theta = \sqrt{\frac{k_{2,\theta}}{k_{E,\theta}}}, \tag{18}$$

where f_{y} is the room temperature 0.2% proof strength and σ_{cr} is the elastic critical buckling stress of the plate at room temperature, calculated as follows:

$$\sigma_{\mathrm{cr}} = k_\sigma \frac{\pi^2 E}{12(1-\nu^2)} \left(\frac{t}{b}\right)^2, \tag{19}$$

in which k_σ is the buckling coefficient determined for the corresponding stress distribution and boundary conditions of the plate [37], ν is the Poisson's ratio and b and t are the plate width and thickness, respectively.

4.3. Cross-section resistance of stainless steel structural elements in fire

Table 6 and Fig. 10 show the calculation of cross-sectional resistances for cross-sections falling into the non-slender and slender classes. As can be seen from the table and figure, in the determination of the axial force and bending moment resistances of stainless steel cross-sections falling into the non-slender class, use of the full cross-section areas A and the plastic section moduli W_{pl} is recommended, while use of the effective cross-section areas A_{eff} and the effective section moduli W_{eff} is recommended for slender sections. The effective section properties A_{eff} and W_{eff} are determined considering the effective widths of the plates constituting the cross-section determined using eqs. (10), (12), (14) and (16) on the basis of the procedure set out in EN 1993-1-5 [37]. It is worth noting that in line with the proposals made herein, the adoption of two section classes using the full and effective cross-section properties was also recommended in [13].

It should be noted that unlike the provisions of the current version of EN 1993-1-2 [3], the proposed cross-section design approach and effective width method utilise the elevated temperature strength and stiffness in the definition of slenderness, which introduces an additional level of complexity. However, consideration of the differential rates of erosion of strength and stiffness in fire leads to more accurate predictions of cross-section capacities, as shown in Section 5. Moreover, this additional complexity can be conservatively avoided by using the maximum values of $\xi_\theta = \sqrt{k_{2,\theta}/k_{E,\theta}}$ for austenitic, duplex and ferritic stainless steel, as given by the expression below, in the predictions of cross-section capacities in the proposed effective width equations given in Section 4.2.

$$\begin{aligned} \xi_{\theta,max} &= \max\left(\sqrt{k_{2,\theta}/k_{E,\theta}}\right) \approx 1.0 \quad \text{for} \quad \text{austenitic and duplex stainless steel,} \\ \xi_{\theta,max} &= \max\left(\sqrt{k_{2,\theta}/k_{E,\theta}}\right) \approx 1.10 \quad \text{for} \quad \text{ferritic stainless steel.} \end{aligned} \tag{20}$$

5. Comparison between EN 1993-1-2 and new effective width method

The accuracy and reliability of the new effective width method for the ultimate strength predictions of stainless steel plates in fire are compared against those of the existing provisions of EN 1993-1-2 [3] in this section, using a large number of results obtained from finite element simulations of stainless steel plates with different edge boundary conditions, elevated temperature levels, stainless steel grades and plate slendernesses. Comparisons are also made against the test results of Uppfelt et al. [39].

5.1. Accuracy assessment

The accuracy of the new effective width method for the prediction of the ultimate resistance of stainless steel plates subjected to axial compression in fire is illustrated in Fig. 11 for hot-rolled stainless steel plates and Fig. 12 for cold-formed stainless steel plates. As can be seen from the figures, the proposed effective width method leads to accurate axial strength predictions for different elevated temperature levels owing to the consideration of the influence of the differential variations in the strength and stiffness at elevated temperatures on the response through the use of the non-dimensional elevated temperature plate buckling slenderness $\overline{\lambda}_{\mathrm{p},\theta}$ in its formulations (see eqs. (10)-(18)). Unlike the effective method of EN 1993-1-2 [3], the new effective method leads to multiple plate buckling curves which results from the use of $\xi_\theta = \sqrt{k_{2,\theta}/k_{E,\theta}}$ in the expression of the plate buckling reduction factors ρ in eqs. (10), (12), (14) and (16), thereby representing the behaviour of stainless steel plates more accurately at different elevated temperature levels. Resistance predictions obtained through the new effective method are compared against those determined through nonlinear finite element modelling in Fig. 13 for hot-rolled stainless steel plates subjected to bending in fire. As can be seen from the figure, although it is less accurate for the prediction of bending moment capacities relative to axial compression resistances, the proposed approach leads to an improved level of accuracy relative to EN 1993-1-2 for the estimations of the ultimate resistances of stainless steel plates in bending.

The accuracy of the new effective width method and EN 1993-1-2 [3] is also compared in Fig. 14 for all stainless steel plates. The results presented in the figure are for internal and outstand stainless steel plates subjected to both pure axial compression and combined bending and axial compression (with the ratios between the edge stresses ψ being equal to 0.5, 0 and -0.5 (i.e. $\psi = 0.5, 0, -0.5$) in the latter loading case), as well as internal plates under pure bending. In Fig. 14, $N_{\mathrm{u,FE}}$ and $M_{\mathrm{u,FE}}$ are the ultimate axial force and bending moment resistances of the stainless steel plates determined using the finite element models, $N_{\mathrm{u,prop}}$ and $M_{\mathrm{u,prop}}$ are the ultimate axial force and bending moment resistances determined using the proposed effective width method and $N_{\mathrm{u,EC3}}$ and $M_{\mathrm{u,EC3}}$ are the ultimate axial force and bending moment resistances predicted using EN 1993-1-2 [3]. As can be seen from Fig. 14, the new effective width method leads to considerably more accurate ultimate strength predictions with a much lower level of scatter for all the internal and outstand plates of different stainless steel grades and with different elevated temperature levels, loading conditions and plate slendernesses $\overline{\lambda}_{\mathrm{p},\theta}$.

The accuracy of the new effective width method and EN 1993-1-2[3] is also assessed in Table 7 and Table 8 by taking into account the mean and the coefficient of variation (COV) of the ratios of the ultimate strength predictions obtained from nonlinear finite element modelling to

those determined through the new effective width method and EN 1993-1-2. As can be seen from the tables, the mean values of the ratios between the ultimate resistances obtained through the finite element models and the proposed effective width method (i.e. $N_{u,FE}/N_{u,prop}$, $M_{u,FE}/M_{u,prop}$ and $N_{u,FE}/N_{u,prop}$ + $M_{u,FE}/M_{u,prop}$) are closer to 1.0 relative to the corresponding mean values of the ratios determined using the EN 1993-1-2 [3] strength predictions (i.e. $N_{u,FE}/N_{u,EC3}$, $M_{u,FE}/M_{u,EC3}$ and $N_{u,FE}/N_{u,EC3}$ + $M_{u,FE}/M_{u,EC3}$) with lower COV values, indicating that the proposed effective width method is able to more accurately predict the ultimate resistances of stainless steel plates in fire relative to EN 1993-1-2 [3].

5.2. Reliability assessment

The reliability of the new effective width method is assessed in Table 9 considering the three reliability criteria put forward by Kruppa [42] for the design of structural steel elements in fire. According to Criterion 1 of [42], none of the strength predictions obtained using the considered design approach should exceed the FE results by more than 15%, while Criterion 2 of [42] states that less than 20% of the design predictions should be on the unsafe side. Finally, Criterion 3 of [42] states that the design predictions should be safe-sided on average. In Table 9, the percentage of the plates for which the overpredictions of resistance exceeded 15% of those obtained from the finite element (FE) models is shown under Criterion 1, the percentage of the plates whose ultimate strengths were overpredicted is shown under Criterion 2 and the average percentage of the differences between the design and FE ultimate strengths is shown under Criterion 3. The violated criteria are highlighted with '*'. As shown in Table 9, the new proposal satisfies all three criteria of Kruppa [42] with the exception of Criterion 2 for the ferritic stainless steel plates in bending, but this is deemed to be acceptable since the reliability criterion is only violated by a very small margin (1.92%) for only one case. The reliability of the existing design provisions of EN 1993-1-2 [3] is also assessed considering the three reliability criteria of Kruppa [42] in Table 10. As can be seen from the table, EN 1993-1-2 [3] violates the reliability criteria of Kruppa [42] for a high number of cases, indicating that the proposed design method provides significantly more reliable ultimate strength predictions for stainless steel plates in fire.

6. Alternative effective width method based on elevated temperature 0.2% proof strength $f_{p0.2,\theta}$

To maintain consistency in the determination of ultimate resistances of stainless steel members with non-slender and slender cross-sections, the elevated temperature material strength at 2% total strain $f_{2,\theta}$ is adopted in the development of the new effective width formulations and in the cross-sectional resistance functions described in Section 4 of this paper. Note that such an approach is in accordance with the upcoming version of EN 1993-1-2 [3] where the elevated temperature material strength at 2% total strain $f_{2,\theta}$ is due to be utilised in the determination of ultimate strengths of carbon steel structural elements in fire regardless of the classes of their cross-sections on the basis of the recent proposals of [13, 43]. In this section, an alternative effective width approach adopting the elevated temperature strength at 0.2% proof strain $f_{p0.2,\theta}$ is presented considering that room temperature design rules in EN 1993-1-4 [4] are primarily based upon 0.2% proof strength $f_{p0.2}$.

6.1. Cross-section classification

In the alternative cross-section classification method based on the elevated temperature 0.2% proof strength $f_{\mathrm{p0.2},\theta}$, cross-sections are again classified as non-slender and slender, similar to the cross-section classification method based on $f_{2,\theta}$ introduced in Subsection 4.1. However, it was observed that use of the elevated temperature 0.2% proof strength $f_{\mathrm{p0.2},\theta}$ leads to overly-conservative ultimate cross-section strength predictions for stocky stainless steel cross-sections in fire. Thus, to accurately predict the cross-section resistances of stocky sections, an additional criteria is introduced herein for the alternative effective width method. According to this additional criteria, if the elevated temperature plate slendernesses of all the constituent plates of a cross-section are less than a secondary threshold slenderness value which is denoted by $\bar{\lambda}_{\mathrm{p0},\theta,s}$, the elevated temperature strength at 2% total strain $f_{2,\theta}$ is used to determine its cross-section resistance. The secondary threshold plate slenderness $\bar{\lambda}_{\mathrm{p0},\theta,s}$ adopted for the use of the elevated temperature material strength at 2% strain in the determination of the cross-section resistances is calculated as:

$$\bar{\lambda}_{\mathrm{p0},\theta,s} = \bar{\lambda}^{*}_{\mathrm{p0},\theta} \sqrt{f_{\mathrm{p0.2},\theta}/f_{2,\theta}}, \tag{21}$$

where $\bar{\lambda}^{*}_{\mathrm{p0},\theta}$ is the threshold plate slendernesses of the new effective width method presented in Section 4 based on $f_{2,\theta}$, determined from eq. (11) for austenitic stainless steel internal elements, eq. (13) for duplex and ferritic stainless steel internal elements, eq. (15) for austenitic stainless steel outstand flanges and eq. (17) for duplex and ferritic stainless steel outstand flanges.

6.2. Alternative effective width method

The alternative effective width formulae based on $f_{\mathrm{p0.2},\theta}$ follow the same format of the new effective width formulae based on $f_{2,\theta}$ presented in Section 4, but the key parameters in the effective formulae have recalibrated to account for the different reference strength using the results from nonlinear finite element modelling. For internal compression elements, the reduction factor for plate buckling for austenitic stainless steel plates is given by:

$$\begin{aligned} \rho &= 1 \qquad\qquad \text{for} \quad \bar{\lambda}_{\mathrm{p},\theta} \leq \bar{\lambda}_{\mathrm{p0},\theta}, \\ \rho &= \frac{0.82}{\left(\bar{\lambda}_{\mathrm{p},\theta}/\sqrt{\xi_\theta}\right)^{0.85}} - \frac{0.04\,(3+\psi)}{\left(\bar{\lambda}_{\mathrm{p},\theta}/\sqrt{\xi_\theta}\right)^{1.7}} \quad \text{for} \quad \bar{\lambda}_{\mathrm{p},\theta} > \bar{\lambda}_{\mathrm{p0},\theta} \end{aligned} \tag{22}$$

with the threshold plate slenderness $\bar{\lambda}_{\mathrm{p0},\theta}$ given by:

$$\bar{\lambda}_{\mathrm{p0},\theta} = \left(0.41 + \sqrt{0.0481 - 0.04\psi}\right)^{1.176} \sqrt{\xi_\theta}. \tag{23}$$

For duplex stainless steel internal plate elements in fire, the plate buckling reduction factor ρ is determined as:

$$\begin{aligned} \rho &= 1 \qquad\qquad \text{for} \quad \bar{\lambda}_{\mathrm{p},\theta} \leq \bar{\lambda}_{\mathrm{p0},\theta}, \\ \rho &= \frac{0.91}{\left(\bar{\lambda}_{\mathrm{p},\theta}/\sqrt{\xi_\theta}\right)^{0.85}} - \frac{0.05\,(3+\psi)}{\left(\bar{\lambda}_{\mathrm{p},\theta}/\sqrt{\xi_\theta}\right)^{1.7}} \quad \text{for} \quad \bar{\lambda}_{\mathrm{p},\theta} > \bar{\lambda}_{\mathrm{p0},\theta} \end{aligned} \tag{24}$$

with

$$\bar{\lambda}_{\mathrm{p0},\theta} = \left(0.455 + \sqrt{0.057 - 0.05\psi}\right)^{1.176} \sqrt{\xi_\theta}, \tag{25}$$

and for ferritic stainless steel internal plate elements, ρ is calculated as:

$$\begin{aligned} \rho &= 1 \qquad \text{for} \quad \bar{\lambda}_{\mathrm{p},\theta} \le \bar{\lambda}_{\mathrm{p0},\theta}, \\ \rho &= \frac{0.86}{\left(\bar{\lambda}_{\mathrm{p},\theta} / \sqrt{\xi_\theta}\right)^{0.85}} - \frac{0.045\,(3+\psi)}{\left(\bar{\lambda}_{\mathrm{p},\theta} / \sqrt{\xi_\theta}\right)^{1.7}} \quad \text{for} \quad \bar{\lambda}_{\mathrm{p},\theta} > \bar{\lambda}_{\mathrm{p0},\theta} \end{aligned} \tag{26}$$

with

$$\bar{\lambda}_{\mathrm{p0},\theta} = \left(0.43 + \sqrt{0.0499 - 0.045\psi}\right)^{1.176} \sqrt{\xi_\theta}. \tag{27}$$

For outstand flanges, the local buckling reduction factor ρ can be calculated for austenitic stainless steel plates as:

$$\begin{aligned} \rho &= 1 \qquad \text{for} \quad \bar{\lambda}_{\mathrm{p},\theta} \le \bar{\lambda}_{\mathrm{p0},\theta}, \\ \rho &= \frac{0.9}{\left(\bar{\lambda}_{\mathrm{p},\theta} / \sqrt{\xi_\theta}\right)^{0.7}} - \frac{0.18}{\left(\bar{\lambda}_{\mathrm{p},\theta} / \sqrt{\xi_\theta}\right)^{1.4}} \quad \text{for} \quad \bar{\lambda}_{\mathrm{p},\theta} > \bar{\lambda}_{\mathrm{p0},\theta} \end{aligned} \tag{28}$$

with

$$\bar{\lambda}_{\mathrm{p0},\theta} = 0.482 \sqrt{\xi_\theta}. \tag{29}$$

For duplex stainless steel outstand flange plates, ρ is calculated as:

$$\begin{aligned} \rho &= 1 \qquad \text{for} \quad \bar{\lambda}_{\mathrm{p},\theta} \le \bar{\lambda}_{\mathrm{p0},\theta}, \\ \rho &= \frac{0.97}{\left(\bar{\lambda}_{\mathrm{p},\theta} / \sqrt{\xi_\theta}\right)^{0.7}} - \frac{0.22}{\left(\bar{\lambda}_{\mathrm{p},\theta} / \sqrt{\xi_\theta}\right)^{1.4}} \quad \text{for} \quad \bar{\lambda}_{\mathrm{p},\theta} > \bar{\lambda}_{\mathrm{p0},\theta} \end{aligned} \tag{30}$$

with

$$\bar{\lambda}_{\mathrm{p0},\theta} = 0.492 \sqrt{\xi_\theta}, \tag{31}$$

and for ferritic stainless steel outstand flange plates, ρ is determined as:

$$\begin{aligned} \rho &= 1 \qquad \text{for} \quad \bar{\lambda}_{\mathrm{p},\theta} \le \bar{\lambda}_{\mathrm{p0},\theta}, \\ \rho &= \frac{0.93}{\left(\bar{\lambda}_{\mathrm{p},\theta} / \sqrt{\xi_\theta}\right)^{0.7}} - \frac{0.2}{\left(\bar{\lambda}_{\mathrm{p},\theta} / \sqrt{\xi_\theta}\right)^{1.4}} \quad \text{for} \quad \bar{\lambda}_{\mathrm{p},\theta} > \bar{\lambda}_{\mathrm{p0},\theta} \end{aligned} \tag{32}$$

with

$$\bar{\lambda}_{\mathrm{p0},\theta} = 0.473 \sqrt{\xi_\theta}, \tag{33}$$

where $\bar{\lambda}_{\mathrm{p},\theta}$ is the elevated temperature plate slenderness calculated as:

$$\bar{\lambda}_{\mathrm{p},\theta} = \xi_\theta \sqrt{\frac{f_\mathrm{y}}{\sigma_\mathrm{cr}}} \quad \text{with} \quad \xi_\theta = \sqrt{\frac{k_{\mathrm{p0.2},\theta}}{k_{\mathrm{E},\theta}}}. \tag{34}$$

6.3. Cross-section resistance

In Table 11 and Fig. 15, the calculation of the cross-section resistances for different classes is illustrated, where the 'non-slender-1' refers to stocky cross-sections whose constituent plates all have elevated temperature plate slenderness values $\overline{\lambda}_{p,\theta}$ less than $\bar{\lambda}_{\mathrm{p0},\theta,s}$. The 'non-slender-2' category represents cross-sections where the non-dimensional plate slenderness of one or more than one constituent plates is greater than $\bar{\lambda}_{\mathrm{p0},\theta,s}$ but the non-dimensional plate slenderness of all the constituent plates is less than $\bar{\lambda}_{\mathrm{p0},\theta}$. Finally, the 'slender' class represents cross-sections where at least one of the constituent plates have plate slenderness values greater than $\bar{\lambda}_{\mathrm{p0},\theta}$. As shown in Table 11 and Fig. 15, for 'non-slender-1' sections, the elevated temperature strength at 2% strain is used in conjunction with the full cross-section properties in the determination of the cross-section resistances, while for 'non-slender-2' and 'slender' sections, the elevated temperature 0.2% proof strength is employed in the determination of the cross-section resistances with full and effective cross-section properties, respectively.

In line with the approach introduced in Section 4.3, the effective width formulations and cross-section classification approach introduced in Section 6.1 and Section 6.2 can be made independent of temperature by conservatively using the maximum value of $\xi_\theta = \sqrt{k_{p,0.2,\theta}/k_{E,\theta}}$ for austenitic, duplex and ferritic stainless steel, as given by the expression below, in the effective width expressions set out in Section 6.2.

$$\xi_{\theta,max} = \max\left(\sqrt{k_{p0.2,\theta}/k_{E,\theta}}\right) \approx 1.0. \tag{35}$$

6.4. Accuracy of the alternative design method based on $f_{\mathrm{p0.2},\theta}$

The alternative effective width method based on the elevated temperature 0.2% proof strength $f_{\mathrm{p0.2},\theta}$ leads to accurate ultimate strength predictions for stainless steel internal and outstand plates subjected to pure compression as shown in Fig. 16 for hot-rolled stainless steel plates and Fig. 17 for cold-formed stainless steel plates. For stocky plates with $\overline{\lambda}_{\mathrm{p},\theta}$ smaller than $\bar{\lambda}_{\mathrm{p0},\theta,s}$, there is an abrupt step in local capacity due to the adoption of the elevated temperature material strength at 2% strain $f_{2,\theta}$ in the determination of the ultimate strengths of these plates. The use of the elevated temperature 0.2% proof strength $f_{\mathrm{p0.2},\theta}$ results in the classification of a higher number of cross-sections as 'non-slender' relative to classification on the basis of the elevated temperature material strength at 2% total strain $f_{2,\theta}$. Thus, the alternative design approach based on $f_{\mathrm{p0.2},\theta}$ leads to a practical way of estimating the ultimate strengths of a higher number stainless steel cross-sections without the need to calculate their effective cross-section properties. However, since (i) the use of the two different reference strengths, $f_{\mathrm{p0.2},\theta}$ and $f_{2,\theta}$, in the determination of the cross-section resistances with two different cross-section plate slenderness limits ($\bar{\lambda}_{\mathrm{p0},\theta,s}$, $\bar{\lambda}_{\mathrm{p0},\theta}$) adds complexity and (ii) the determination of the effective width properties of stainless steel cross-sections can be readily automated within design software, the use of the new effective width method and cross-section classification rules based on the elevated temperature strength at 2% total strain $f_{2,\theta}$ introduced in Section 4 is recommended herein. Both the new and alternative effective width methods adopting $f_{2,\theta}$ and $f_{\mathrm{p0.2},\theta}$ are presented in this paper since each have relative merits.

7. Conclusions

The current provisions of the European structural steel fire design standard EN 1993-1-2 [3] directs the designer to EN 1993-1-4 [4] for the local buckling assessment of stainless steel plates in fire. However, since the plate buckling design rules of EN 1993-1-4 [4] were originally developed considering the room temperature response of stainless steel plates, they lead to inaccurate predictions of ultimate strength in fire due to (i) failure to reflect the material stress-strain response of stainless steel in fire and (ii) the neglect of the different rates of strength and stiffness erosion of stainless steel at elevated temperatures. To enable accurate predictions of the response of stainless steel plates at elevated temperatures, a new effective width method is proposed in this study. Unlike the current provisions of EN 1993-1-2 [3], in the new effective width method, temperature-dependent plate slenderness $\bar{\lambda}_{p,\theta}$ is employed in conjunction with new plate buckling curves to determine the effective widths of stainless steel plates in fire. It was shown that the new effective width method leads to more accurate and reliable ultimate strength predictions relative to the current design rules of EN 1993-1-2 [3] as assessed against results obtained from nonlinear finite element modelling of stainless steel plates of different grades for a range of elevated temperature levels, loading conditions, boundary conditions and local slendernesses. In conjunction with the new effective width method, new cross-section classification rules were also introduced for stainless steel cross-sections in fire, adopting two distinct classes, referred to as 'non-slender' and 'slender', whose ultimate cross-section resistances are determined using the full and effective cross-section properties, respectively. The proposed method for the treatment of local buckling of stainless steel plates in fire based on the elevated temperature strength at 2% strain $f_{2,\theta}$ described in Section 4 of the current paper is due to be incorporated into the upcoming version of Eurocode 3: Part 1.2.

Acknowledgement

Financial support for the first author was provided by the China Scholarship Council.

References

[1] Gardner, L.. Stability and design of stainless steel structures–Review and outlook. Thin-Walled Structures 2019;141:208–216.

[2] Wang, F.C. and Han, L.H.. Analytical behavior of carbon steel-concrete-stainless steel double-skin tube (DST) used in submarine pipeline structure. Marine Structures 2019; 63:99–116.

[3] EN 1993-1-2, Eurocode 3 Design of Steel Structures–Part 1-2: General Rules–Structural Fire Design. European Committee for Standardization (CEN), Brussels; 2005.

[4] EN 1993-1-4, Eurocode 3 Design of steel structures–Part 1-4: General rules–Supplementary rules for stainless steels. European Committee for Standardization (CEN), Brussels; 2015.

[5] Ng, K.T. and Gardner, L.. Buckling of stainless steel columns and beams in fire. Engineering Structures 2007;29(5):717–730.

[6] Gardner, L.. Stainless steel structures in fire. Proceedings of the Institution of Civil Engineers–Structures and Buildings 2007;160:129–138.

[7] Fan, S., Ding, X., Sun, W., Zhang, L. and Liu, M., Experimental investigation on fire resistance of stainless steel columns with square hollow section. Thin-Walled Structures 2016;98:196–211.

[8] Fan, S., Liu, M., Sun, W., Guo, Y. and Han, Y.L.. Experimental investigation of eccentrically compressed stainless steel columns with constraints in fire. Fire Safety Journal 2018;99:49–62.
[9] Ding, R., Fan, S., Chen, G., Li, C., Du, E. and Liu, C.. Fire resistance design method for restrained stainless steel H-section columns under axial compression. Fire Safety Journal 2019;108:102837.
[10] Mohammed, A. and Afshan, S.. Numerical modelling and fire design of stainless steel hollow section columns. Thin-Walled Structures 2019;144:106243.
[11] Ranby, A.. Structural fire design of thin walled steel sections. Journal of Constructional Steel Research 1998;1(46):303–304.
[12] Renaud, C. and Zhao, B.. Investigation of simple calculation method in EN 1993-1-2 for buckling of hot rolled class 4 steel members exposed to fire. In Fourth International Workshop "Structures in Fire" 2006;199–211.
[13] Couto, C., Real, P.V., Lopes, N. and Zhao, B.. Effective width method to account for the local buckling of steel thin plates at elevated temperatures. Thin-Walled Structures 2014;84:134–149.
[14] Knobloch, M. and Fontana, M.. Strain-based approach to local buckling of steel sections subjected to fire. Journal of Constructional Steel Research 2006;62(1-2):44–67.
[15] Selamet, S. and Garlock, M.E.. Plate buckling strength of steel wide-flange sections at elevated temperatures. Journal of Structural Engineering, ASCE 2012;139(11):1853–1865.
[16] ABAQUS v.6.14 Reference Manual. Simulia, Dassault Systemes;2014.
[17] Trahair, N.S., Bradford, M.A., Nethercot, D.A. and Gardner, L.. The behaviour and design of steel structures to EC3, Fourth Edition. CRC Press, 2008.
[18] Gardner, L., Fieber, A. and Macorini, L.. Formulae for calculating elastic local buckling stresses of full structural cross-sections. Structures 2019;17:2–20.
[19] Fieber, A., Gardner, L. and Macorini, L.. Formulae for determining elastic local buckling half-wavelengths of structural steel cross-sections. Journal of Constructional Steel Research 2019;159:493–506.
[20] Kucukler, M., Gardner, L. and Macorini, L.. Flexural-torsional buckling assessment of steel beam–columns through a stiffness reduction method. Engineering Structures 2015;101:662–676.
[21] Kucukler, M., Gardner, L. and Macorini, L.. Lateral-torsional buckling assessment of steel beams through a stiffness reduction method. Journal of Constructional Steel Research 2015;109:87–100.
[22] Zhang, L., Tan, K.H. and Zhao, O.. Experimental and numerical studies of fixed-ended cold-formed stainless steel equal-leg angle section columns. Engineering Structures 2019;184:134–144.
[23] He, A., Liang, Y., Zhao, O.. Experimental and numerical studies of austenitic stainless steel CHS stub columns after exposed to elevated temperatures. Journal of Constructional Steel Research 2019;154:293—305.
[24] Kucukler, M. and Gardner, L.. Design of web-tapered steel beams against lateral-torsional buckling through a stiffness reduction method. Engineering Structures 2019;190:246–261.
[25] Arrayago, I., Real, E. and Gardner, L.. Description of stress–strain curves for stainless steel alloys. Materials & Design 2015;87:540–552.
[26] Rasmussen, K.J.. Full-range stress-strain curves for stainless steel alloys. Journal of Constructional Steel Research 2003;59(1):47–61.
[27] Mirambell, E. and Real, E.. On the calculation of deflections in structural stainless steel beams: an experimental and numerical investigation. Journal of Constructional Steel Research 2000;54(1):109–133.
[28] Kucukler, M., Xing, Z., Gardner, L.. Behaviour and design of stainless steel I-section columns in fire, Journal of Constructional Steel Research 2019; Submitted for publication.
[29] Liang, Y., Manninen, T., Zhao, O., Walport, F. and Gardner, L.. Elevated temperature material properties of a new high-chromium austenitic stainless steel, Journal of Constructional Steel Research 2019;152:261–273.
[30] Afshan, S., Zhao, O. and Gardner, L.. Standardised material properties for numerical parametric studies of stainless steel structures and buckling curves for tubular columns. Journal of Constructional Steel Research 2009;152:2–11.
[31] Design manual for structural stainless steel, Fourth Edition, Steel Construction Institute (SCI);2017.
[32] Gardner, L., Insausti, A., Ng, K.T. and Ashraf, M.. Elevated temperature material properties of stainless steel alloys. Journal of Constructional Steel Research 2010;66(5):634–647.
[33] Gardner, L., Bu, Y., Francis, P., Baddoo, N.R., Cashell, K.A. and McCann, F.. Elevated temperature material properties of stainless steel reinforcing bar. Construction and Building Materials 2016;114:977–997.

[34] Chen, J. and Young, B.. Stress–strain curves for stainless steel at elevated temperatures. Engineering Structures 2006;28(2):229–239.
[35] Ala-Outinen, T., Oksanen, T.. Stainless steel compression members exposed to fire, Research Notes 1864, Technical Research Centre of Finland (VTT), Finland; 1997.
[36] Timoshenko, S.P. and Gere, J.M. Theory of Elastic Stability. McGraw-Hill., New York. 1961.
[37] EN 1993-1-5, Eurocode 3 Design of steel structures-Part 1-5: Plated structural elements, European Committee for Standardization (CEN), Brussels; 2005.
[38] Jandera, M., Gardner, L. and Machacek, J.. Residual stresses in cold-rolled stainless steel hollow sections. Journal of Constructional Steel Research 2008;64(11):1255–1263.
[39] Uppfeldt, B., Outinen, T.A. and Veljkovic, M.. A design model for stainless steel box columns in fire. Journal of Constructional Steel Research 2008;64(11):1294–1301.
[40] Gardner, L. and Baddoo, N.R.. Fire testing and design of stainless steel structures. Journal of Constructional Steel Research 2006;62(6):532–543.
[41] Gardner, L. and Theofanous, M.. Discrete and continuous treatment of local buckling in stainless steel elements. Journal of Constructional Steel Research 2008;64(11):1207–1216.
[42] Kruppa, J.. Eurocodes-fire parts: Proposal for a methodology to check the accuracy of assessment methods. CEN TC 250, Horizontal Group Fire, Document no: 99/130; 1999.
[43] Couto, C., Real, P.V., Lopes, N., and Zhao, B.. Resistance of steel cross-sections with local buckling at elevated temperatures. Journal of Constructional Steel Research 2015;109:101–114.

8. Figures

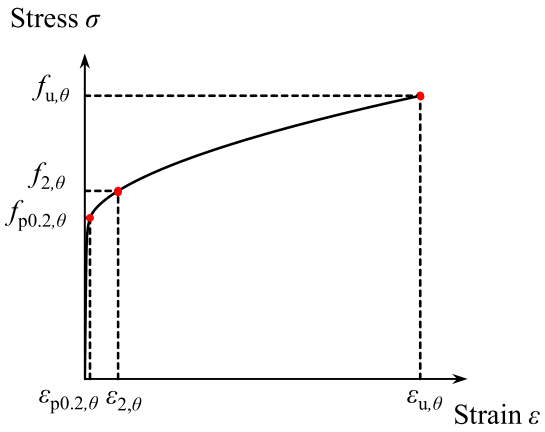

Figure 1: Two-stage elevated temperature Ramberg-Osgood material model [25–27] adopted in FE models

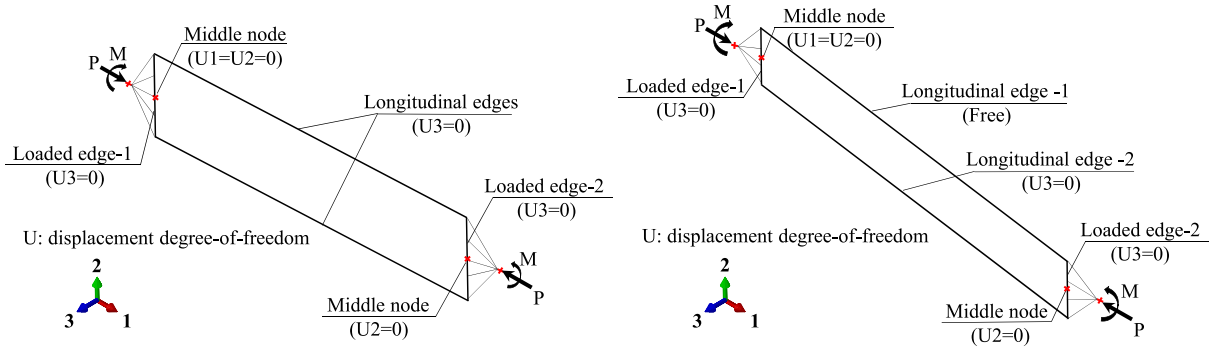

(a) Internal element

(b) Outstand flange

Figure 2: Boundary conditions applied to the FE models of stainless steel internal elements and outstand flanges

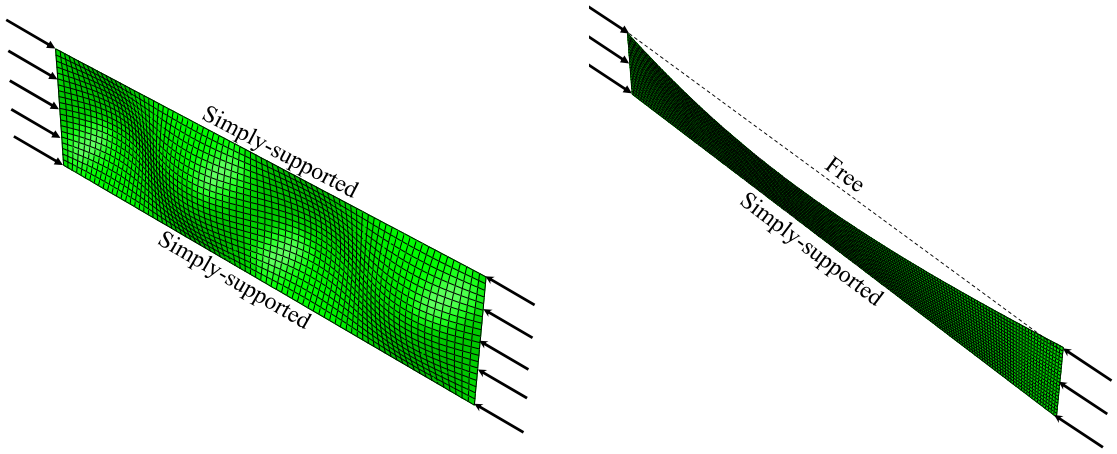

Figure 3: Lowest eigenmodes for internal elements (left) and outstand flanges (right) used to apply geometrical imperfections in subsequent nonlinear analyses

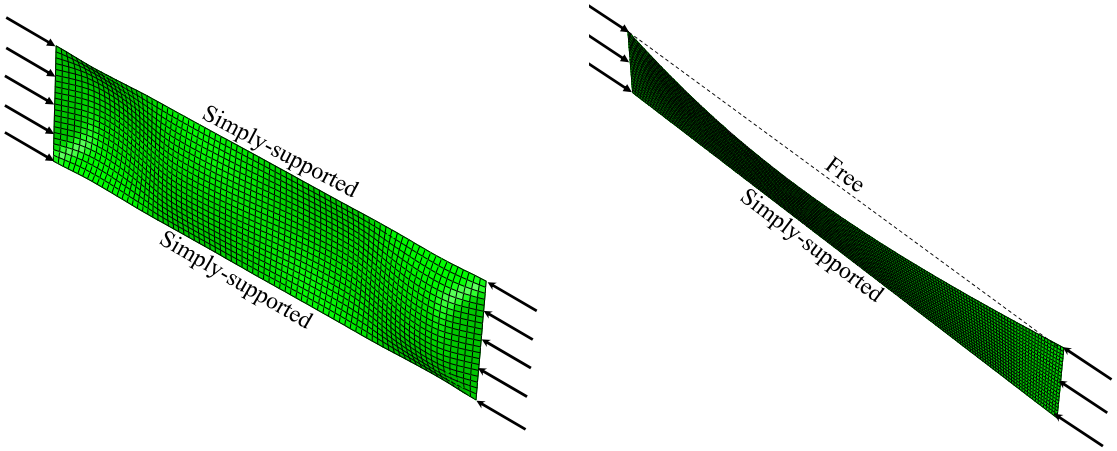

Figure 4: Typical failure modes of compressed internal elements (left) and outstand flanges (right) in fire

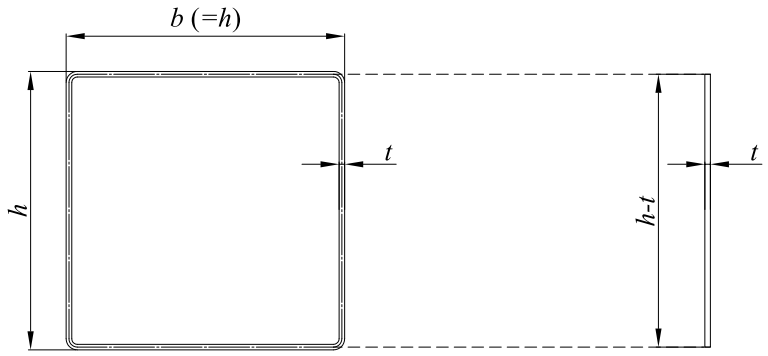

Figure 5: Definition of plate dimensions used in validation of numerical plate FE models against experiments performed by Uppfeldt et al. [39] on stainless steel SHS in fire

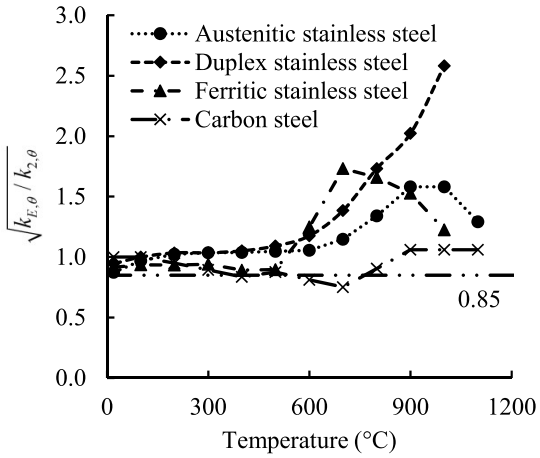

Figure 6: Variation of $\sqrt{k_{E,\theta}/k_{2,\theta}}$ for austenitic, duplex and ferritic stainless steel and carbon steel at different elevated temperature levels

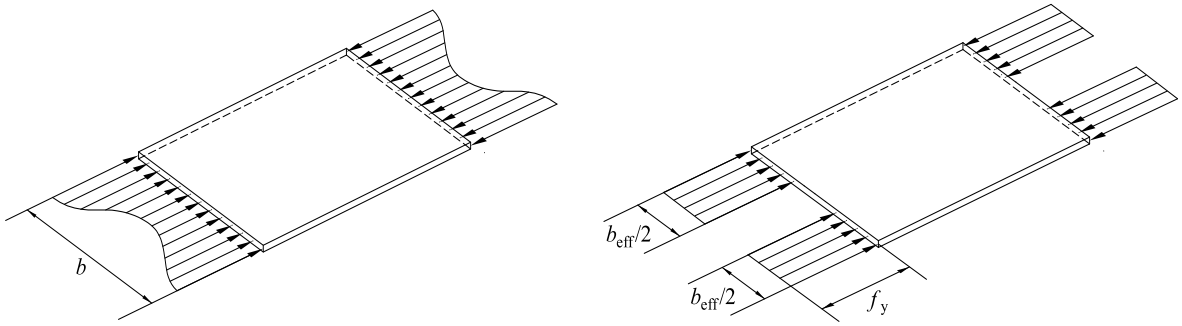

(a) Axial post-buckling stress distribution in a simply-supported plate

(b) Effective width method

Figure 7: Axial post-buckling stress distribution in a simply-supported plate and effective width method

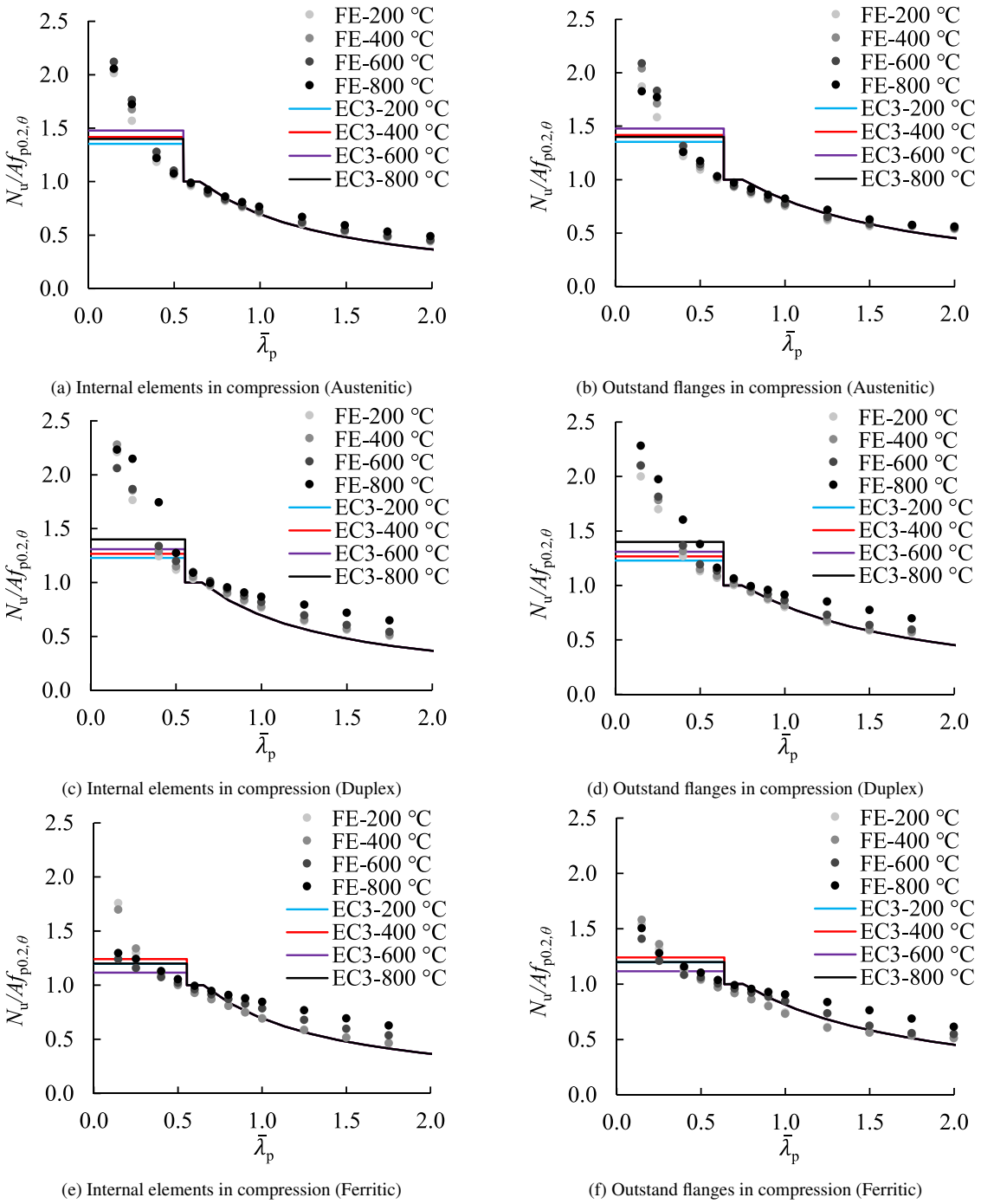

(a) Internal elements in compression (Austenitic)

(b) Outstand flanges in compression (Austenitic)

(c) Internal elements in compression (Duplex)

(d) Outstand flanges in compression (Duplex)

(e) Internal elements in compression (Ferritic)

(f) Outstand flanges in compression (Ferritic)

Figure 8: Assessment of EN 1993-1-2 [3] against FE results for the local buckling strength predictions of hot-rolled stainless steel plates subjected to axial compression

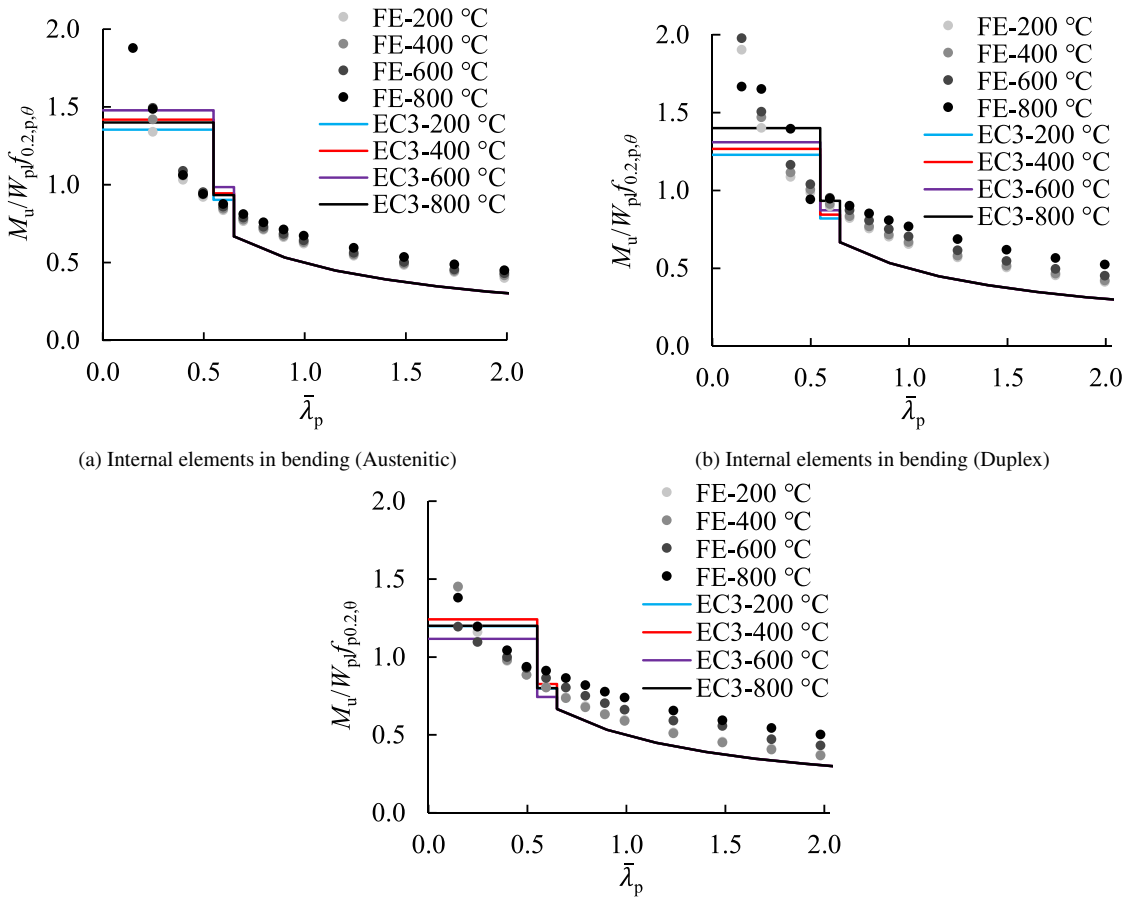

(a) Internal elements in bending (Austenitic)

(b) Internal elements in bending (Duplex)

(c) Internal elements in bending (Ferritic)

Figure 9: Assessment of EN 1993-1-2 [3] against FE results for the local buckling strength predictions of hot-rolled stainless steel plates subjected to bending

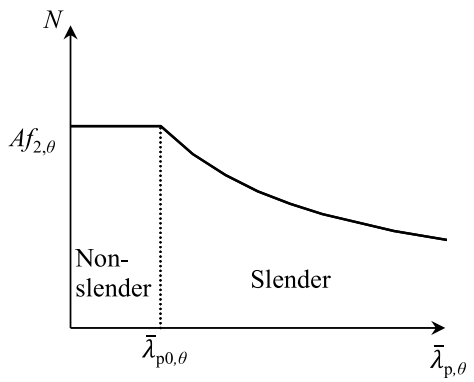

(a) Plates in compression

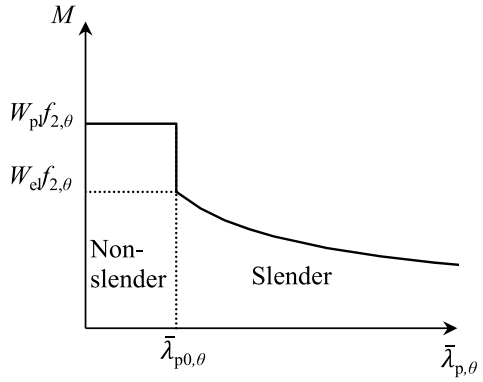

(b) Plates in bending

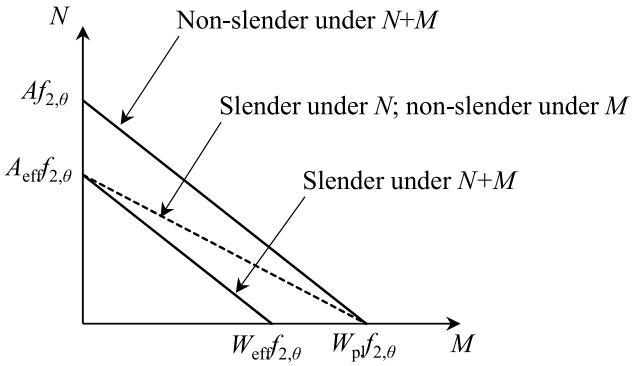

(c) Plates under combined compression and bending

Figure 10: Cross-sectional resistances in new design method based on $f_{2,\theta}$

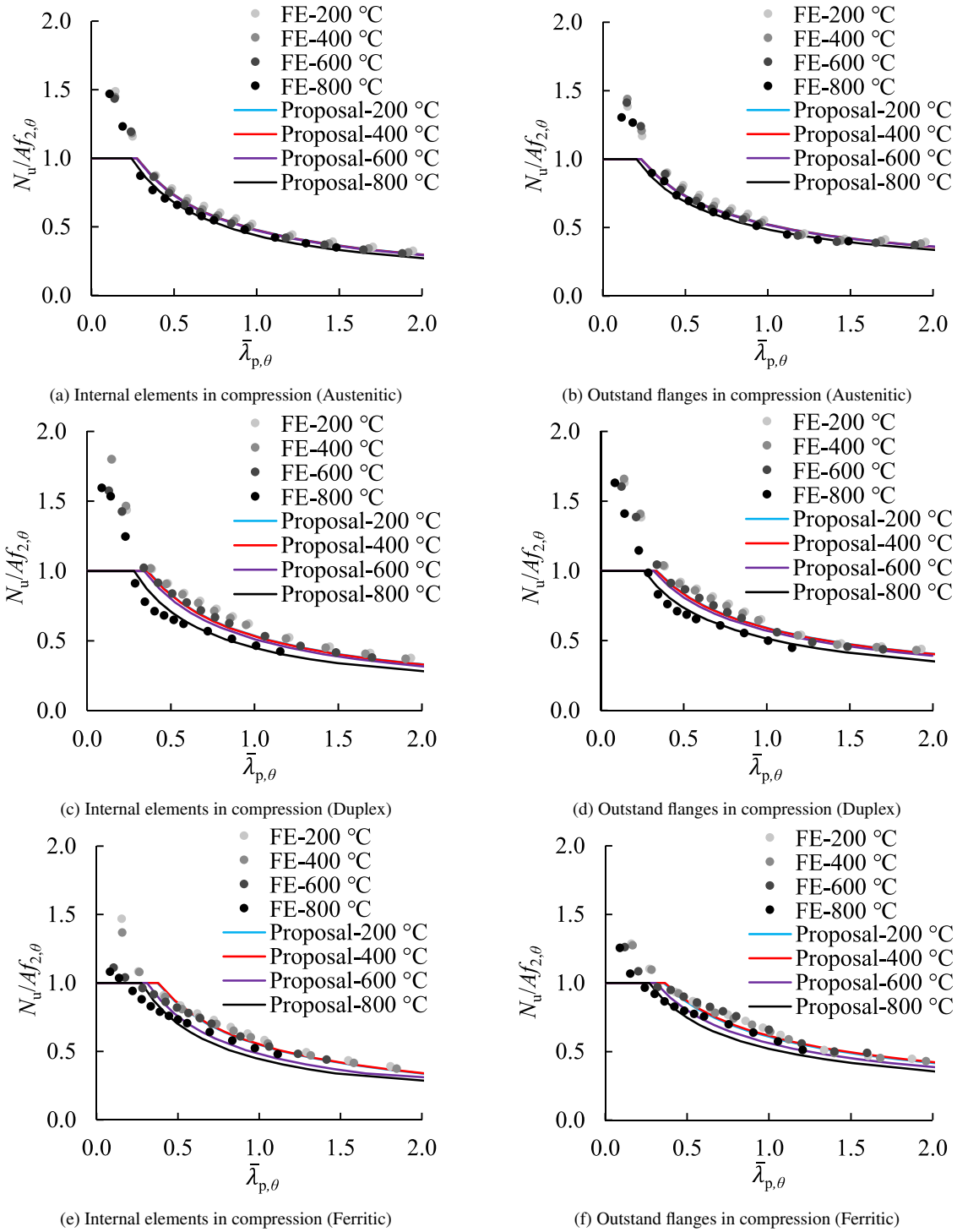

(a) Internal elements in compression (Austenitic)

(b) Outstand flanges in compression (Austenitic)

(c) Internal elements in compression (Duplex)

(d) Outstand flanges in compression (Duplex)

(e) Internal elements in compression (Ferritic)

(f) Outstand flanges in compression (Ferritic)

Figure 11: Assessment of new design method based on $f_{2,\theta}$ against FE results for the local buckling strength predictions of hot-rolled stainless steel plates

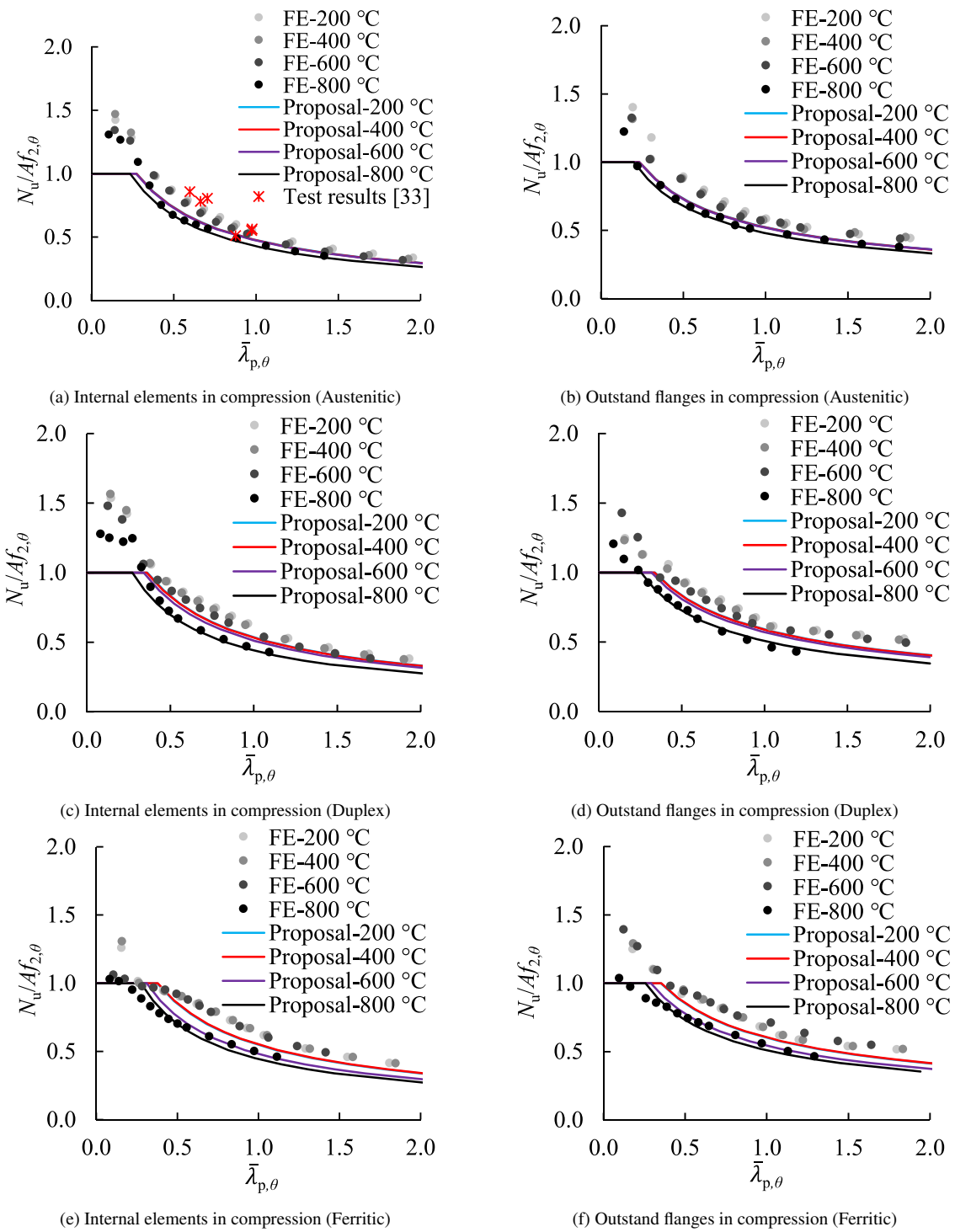

(a) Internal elements in compression (Austenitic)

(b) Outstand flanges in compression (Austenitic)

(c) Internal elements in compression (Duplex)

(d) Outstand flanges in compression (Duplex)

(e) Internal elements in compression (Ferritic)

(f) Outstand flanges in compression (Ferritic)

Figure 12: Assessment of new design method based on $f_{2,\theta}$ against FE results for the local buckling strength predictions of cold-formed stainless steel plates

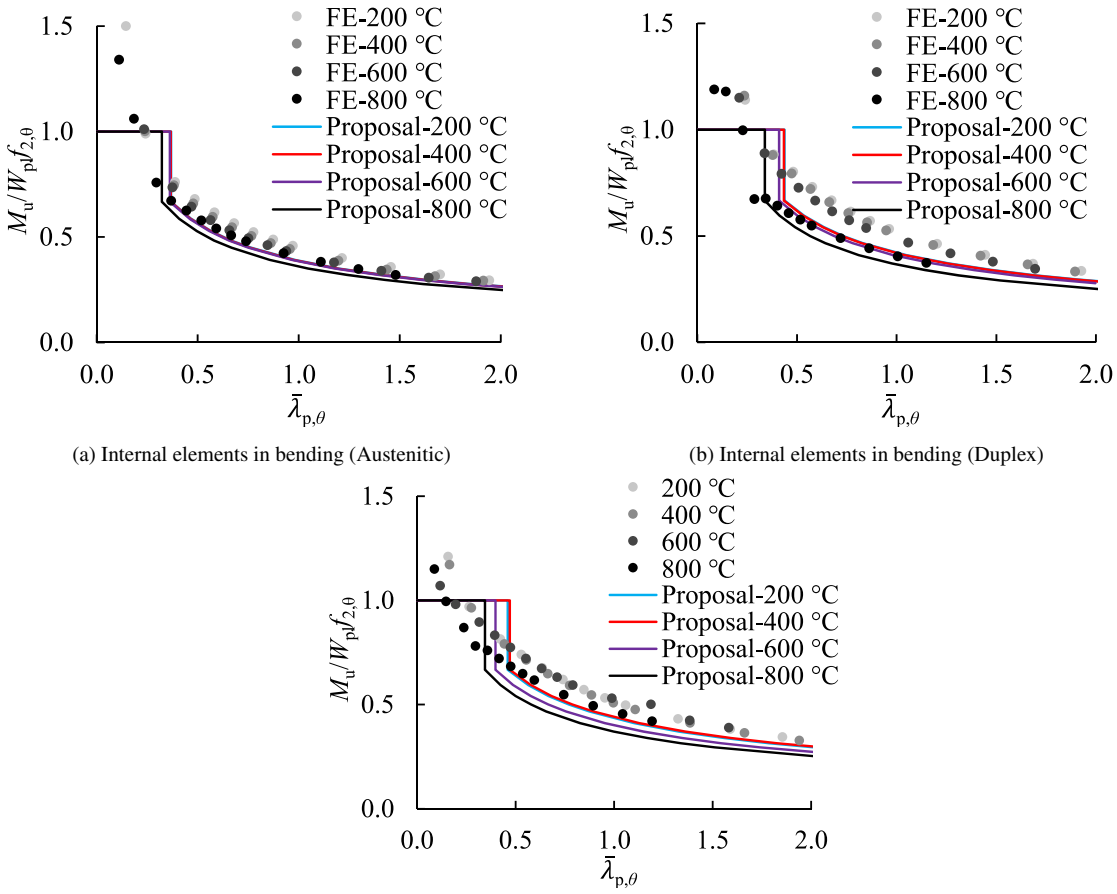

(a) Internal elements in bending (Austenitic)

(b) Internal elements in bending (Duplex)

(c) Internal elements in bending (Ferritic)

Figure 13: Assessment of new design method based on $f_{2,\theta}$ against FE results for the local buckling strength predictions of hot-rolled stainless steel plates subjected to bending

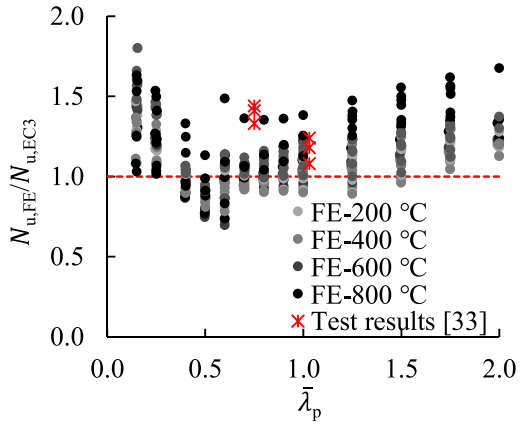

(a) Assessment of EN 1993-1-2 for stainless steel plates in compression

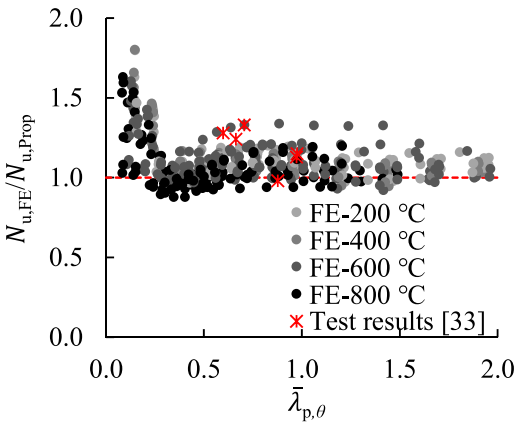

(b) Assessment of new proposal for stainless steel plates in compression

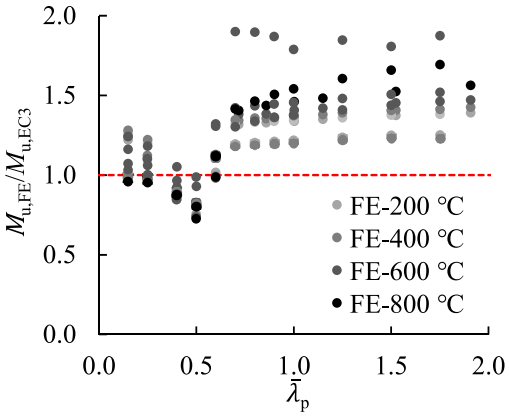

(c) Assessment of EN 1993-1-2 for stainless steel plates in bending

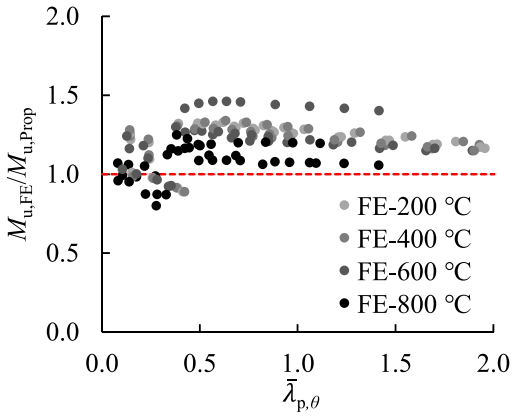

(d) Assessment of new proposal for stainless steel plates in bending

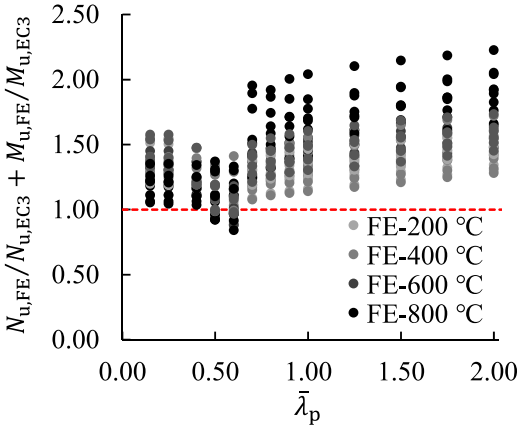

(e) Assessment of EN 1993-1-2 for stainless steel plates under combined axial compression and bending

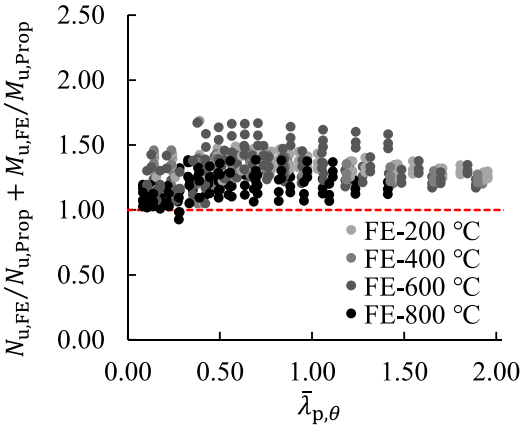

(f) Assessment of new proposal for stainless steel plates under combined axial compression and bending

Figure 14: Assessment of EN 1993-1-2 [3] and new proposal against FE results for all stainless steel plates

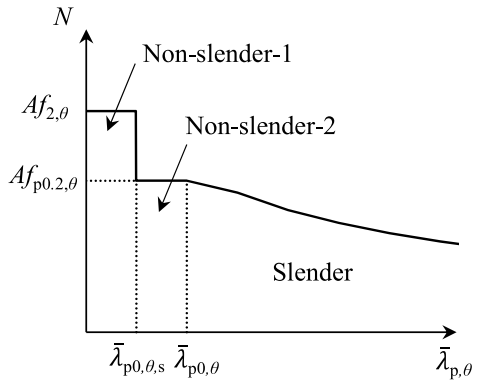

(a) Plates in compression

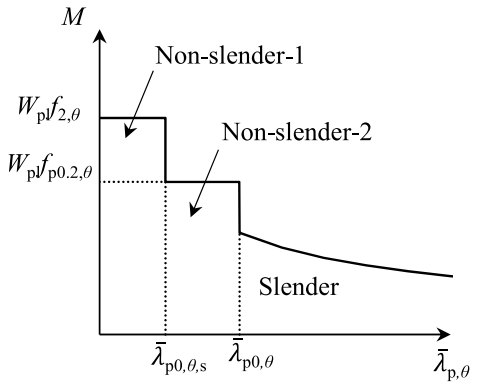

(b) Plates in bending

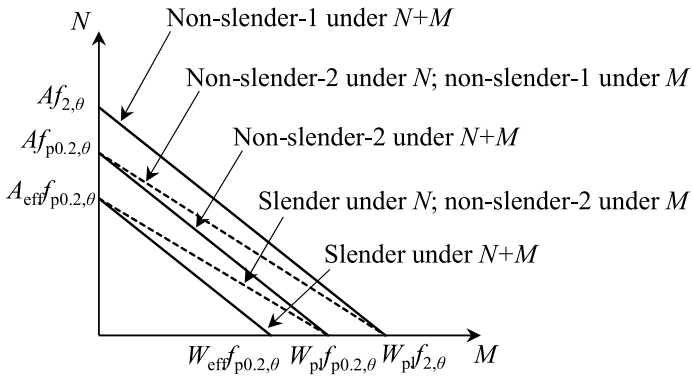

(c) Plates under combined compression and bending

Figure 15: Cross-sectional resistances in alternative design method based on $f_{\mathrm{p0.2},\theta}$

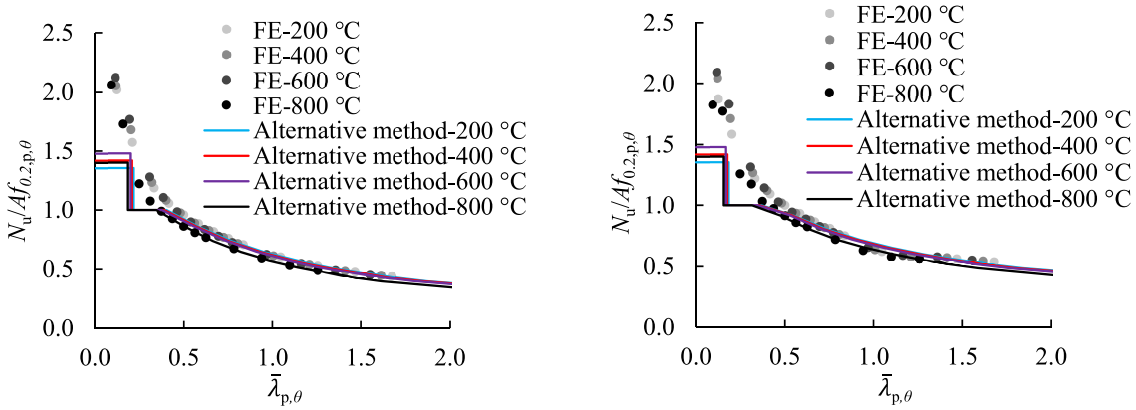

(a) Internal elements in compression (Austenitic)

(b) Outstand flanges in compression (Austenitic)

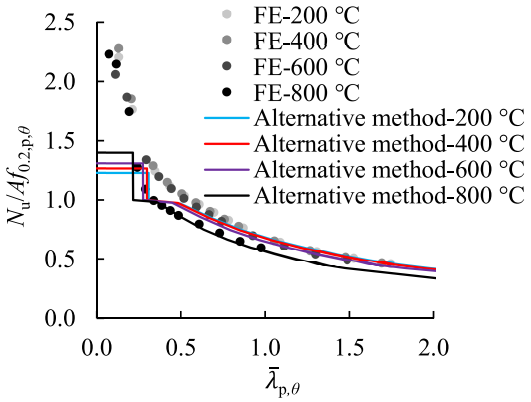

(c) Internal elements in compression (Duplex)

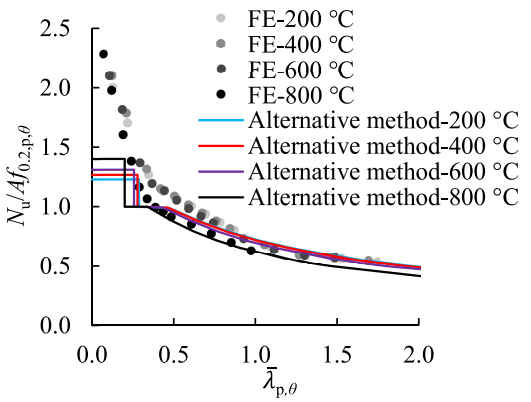

(d) Outstand flanges in compression (Duplex)

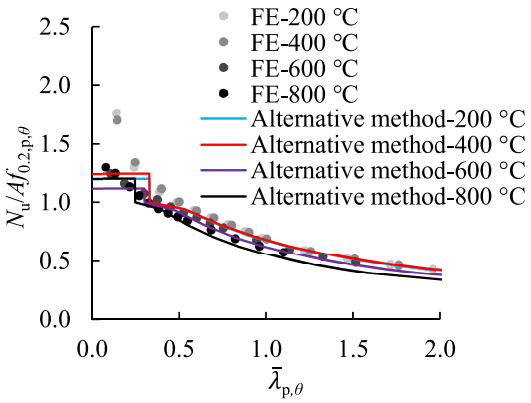

(e) Internal elements in compression (Ferritic)

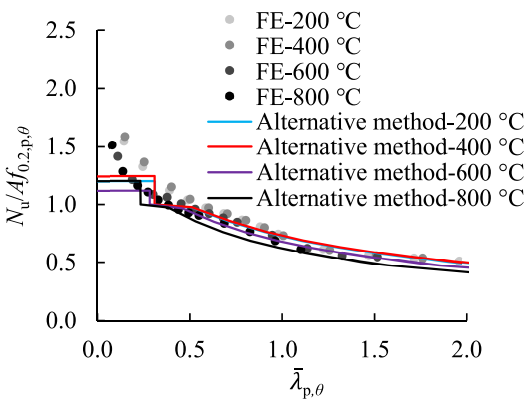

(f) Outstand flanges in compression (Ferritic)

Figure 16: Assessment of alternative effective width method based on $f_{p0.2,\theta}$ against FE results for the local buckling strength predictions of hot-rolled stainless steel plates

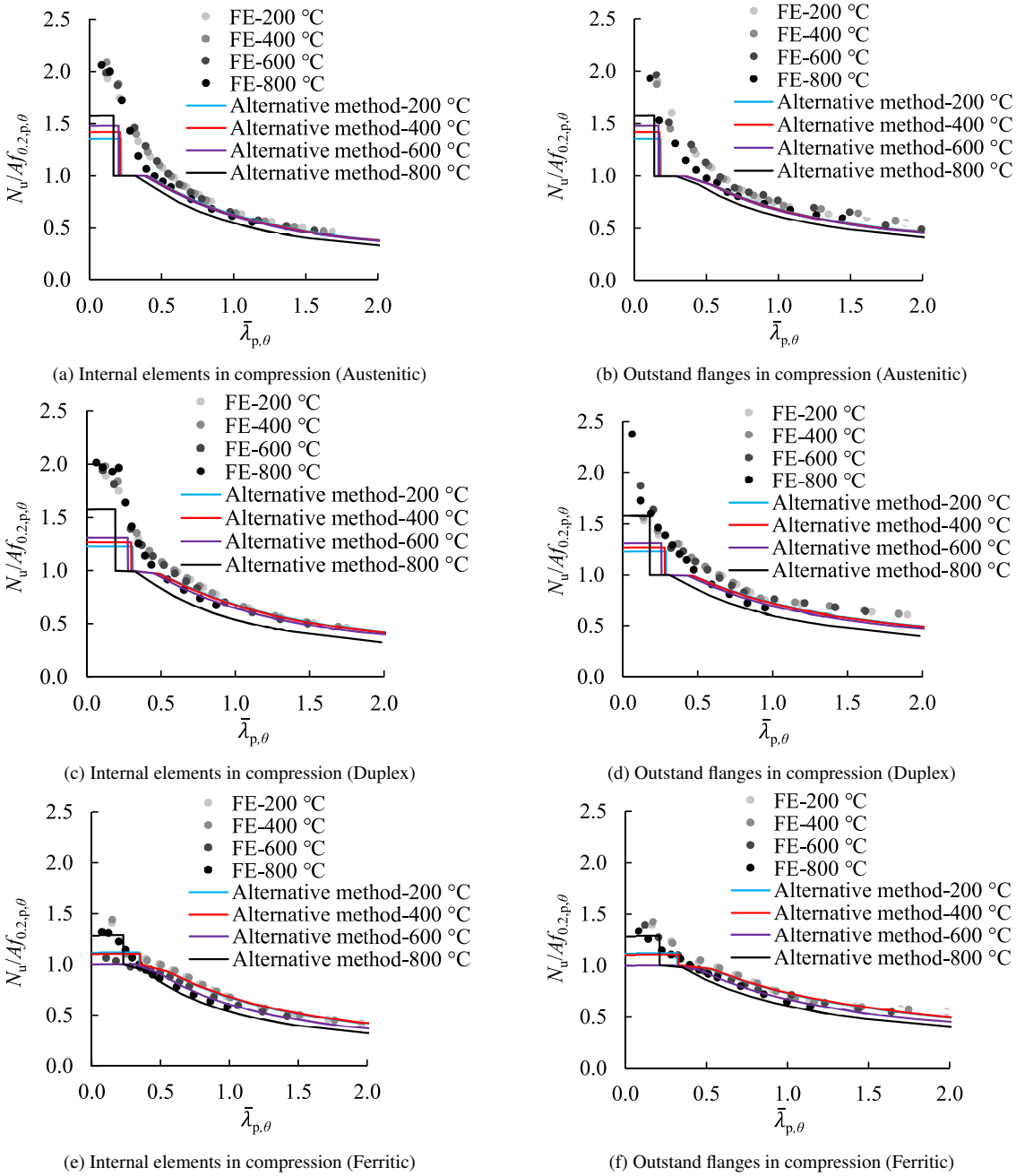

(a) Internal elements in compression (Austenitic)

(b) Outstand flanges in compression (Austenitic)

(c) Internal elements in compression (Duplex)

(d) Outstand flanges in compression (Duplex)

(e) Internal elements in compression (Ferritic)

(f) Outstand flanges in compression (Ferritic)

Figure 17: Assessment of alternative effective width method based on $f_{p0.2,\theta}$ against FE results for the local buckling strength predictions of cold-formed stainless steel plates

9. Tables

Table 1: Summary of room temperature material properties for austenitic, duplex and ferritic stainless steel grades used in this study

Material properties used for hot-rolled plates					
Material grade	E (GPa)	f_y (MPa)	f_u (MPa)	ε_u	$n_\theta(=n)$
Austenitic	200	280	580	0.50	9.1
Duplex	200	530	770	0.30	9.3
Ferritic	200	320	480	0.16	17.2
Material properties used for cold-formed plates					
Material grade	E (GPa)	f_y (MPa)	f_u (MPa)	ε_u	$n_\theta(=n)$
Austenitic	200	460	700	0.20	7.1
Duplex	200	630	780	0.13	7.5
Ferritic	200	430	490	0.06	11.5

Table 2: Comparison of ultimate strengths of stainless steel plates obtained from physical experiments by [39] and from FE analyses in this study

Section	f_y (20 °C) (MPa)	Temp. (°C)	$N_{u,test}$ (kN)	$N_{u,FE}$ (kN)	$N_{u,FE}/N_{u,test}$
SHS 200×200×5	360	609	176	169	0.96
SHS 200×200×5	360	685	144	145	1.01
SHS 200×200×5	360	764	118	115	0.98
SHS 150×150×3	405	676	51	57	1.11
SHS 150×150×3	405	720	42	48	1.16
SHS 150×150×3	405	588	63	62	0.99

Table 3: Comparison of ultimate bending moments of stainless steel beams obtained from physical experiments by [40] and from FE analyses in this study

Cross-section	f_y (20 °C) (MPa)	Temp. (°C)	$M_{u,test}$ (kNm)	$M_{u,FE}$ (kNm)	$M_{u,FE}/M_{u,test}$
RHS-200×125×6	262	884	27.8	26.4	0.95
I-200×150×6	262	944	17.2	17.4	1.01
I-120×64	275	650	15.2	14.4	0.95

Table 4: Width-to-thickness limits for plate classification at room temperature

Element	Class 1	Class 2	Class 3
Internal element subjected to compression	33ε	35ε	37ε
Internal element subjected to bending	72ε	76ε	90ε
Outstand flanges subjected to compression	9ε	10ε	14ε

Table 5: Determination of cross-sectional resistances in EN 1992-1-2 [3]

Cross-section classification	Design resistance in compression	Design resistance in bending
Class 1 and 2	$N_{\mathrm{fi,t,Rd}} = A f_{2,\theta}/\gamma_{\mathrm{M,fi}}$	$M_{\mathrm{fi,t,Rd}} = W_{\mathrm{pl}} f_{2,\theta}/\gamma_{\mathrm{M,fi}}$
Class 3	$N_{\mathrm{fi,t,Rd}} = A f_{2,\theta}/\gamma_{\mathrm{M,fi}}$	$M_{\mathrm{fi,t,Rd}} = W_{\mathrm{el}} f_{2,\theta}/\gamma_{\mathrm{M,fi}}$
Class 4	$N_{\mathrm{fi,t,Rd}} = A_{\mathrm{eff}} f_{\mathrm{p0.2},\theta}/\gamma_{\mathrm{M,fi}}$	$M_{\mathrm{fi,t,Rd}} = W_{\mathrm{eff}} f_{\mathrm{p0.2},\theta}/\gamma_{\mathrm{M,fi}}$

Table 6: Definition of cross-sectional resistances in new design method based on $f_{2,\theta}$

Cross-section classification	Design resistance in compression	Design resistance in bending
Non-slender	$N_{\mathrm{fi,t,Rd}} = A f_{2,\theta}/\gamma_{\mathrm{M,fi}}$	$M_{\mathrm{fi,t,Rd}} = W_{\mathrm{pl}} f_{2,\theta}/\gamma_{\mathrm{M,fi}}$
Slender	$N_{\mathrm{fi,t,Rd}} = A_{\mathrm{eff}} f_{2,\theta}/\gamma_{\mathrm{M,fi}}$	$M_{\mathrm{fi,t,Rd}} = W_{\mathrm{eff}} f_{2,\theta}/\gamma_{\mathrm{M,fi}}$

Table 7: Accuracy assessment of new design proposals

Plates in compression			
$N_{u,FE}/N_{u,prop}$	Austenitic	Duplex	Ferritic
Mean	1.100	1.146	1.101
COV	0.105	0.154	0.096
Plates in bending			
$M_{u,FE}/M_{u,prop}$	Austenitic	Duplex	Ferritic
Mean	1.182	1.183	1.198
COV	0.080	0.094	0.150
Plates in combined axial compression and bending			
$N_{u,FE}/N_{u,prop} + M_{u,FE}/M_{u,prop}$	Austenitic	Duplex	Ferritic
Mean	1.297	1.293	1.294
COV	0.095	0.085	0.120

Table 8: Accuracy assessment of EN 1993-1-2 [3]

Plates in compression			
$N_{u,FE}/N_{u,EC3}$	Austenitic	Duplex	Ferritic
Mean	1.069	1.181	1.057
COV	0.162	0.173	0.155
Plates in bending			
$M_{u,FE}/M_{u,EC3}$	Austenitic	Duplex	Ferritic
Mean	1.250	1.346	1.207
COV	0.205	0.216	0.196
Plates in combined axial compression and bending			
$N_{u,FE}/N_{u,EC3} + M_{u,FE}/M_{u,EC3}$	Austenitic	Duplex	Ferritic
Mean	1.315	1.412	1.297
COV	0.154	0.177	0.161

Table 9: Reliability assessment of new design proposals

Plates in compression			
$N_{u,FE}/N_{u,prop}$	Austenitic	Duplex	Ferritic
Criterion 1	0.00	0.00	0.00
Criterion 2	11.49	8.91	15.38
Criterion 3	-8.25	-11.01	-8.43
Plates in bending			
$M_{u,FE}/M_{u,prop}$	Austenitic	Duplex	Ferritic
Criterion 1	0.00	0.00	1.92*
Criterion 2	5.77	9.62	20.00
Criterion 3	-14.80	-14.61	-14.47
Plates in combined axial compression and bending			
$N_{u,FE}/N_{u,prop} + M_{u,FE}/M_{u,prop}$	Austenitic	Duplex	Ferritic
Criterion 1	0.00	0.00	0.00
Criterion 2	0.52	0.00	0.93
Criterion 3	-29.66	-29.31	-29.25

Table 10: Reliability assessment of EN 1993-1-2 [3]

Plates in compression			
$N_{u,FE}/N_{u,EC3}$	Austenitic	Duplex	Ferritic
Criterion 1	8.91*	1.72*	5.70*
Criterion 2	35.34*	12.93*	45.30*
Criterion 3	-3.98	-13.01	-3.32
Plates in bending			
$M_{u,FE}/M_{u,EC3}$	Austenitic	Duplex	Ferritic
Criterion 1	13.46*	5.77*	5.77*
Criterion 2	25.00*	13.46	25.00*
Criterion 3	-15.75	-22.06	-13.89
Plates in combined axial compression and bending			
$N_{u,FE}/N_{u,EC3} + M_{u,FE}/M_{u,EC3}$	Austenitic	Duplex	Ferritic
Criterion 1	0.52*	0.00	0.51*
Criterion 2	9.90	3.08	6.67
Criterion 3	-31.54	-41.15	-29.15

Table 11: Definition of cross-sectional resistances in alternative design method based on $f_{\mathrm{p0.2},\theta}$

Cross-section classification	Design resistance in compression	Design resistance in bending
Non-slender-1	$N_{\mathrm{fi,t,Rd}} = A f_{2,\theta}/\gamma_{\mathrm{M,fi}}$	$M_{\mathrm{fi,t,Rd}} = W_{\mathrm{pl}} f_{2,\theta}/\gamma_{\mathrm{M,fi}}$
Non-slender-2	$N_{\mathrm{fi,t,Rd}} = A f_{\mathrm{p0.2},\theta}/\gamma_{\mathrm{M,fi}}$	$M_{\mathrm{fi,t,Rd}} = W_{\mathrm{pl}} f_{\mathrm{p0.2},\theta}/\gamma_{\mathrm{M,fi}}$
Slender	$N_{\mathrm{fi,t,Rd}} = A_{\mathrm{eff}} f_{\mathrm{p0.2},\theta}/\gamma_{\mathrm{M,fi}}$	$M_{\mathrm{fi,t,Rd}} = W_{\mathrm{eff}} f_{\mathrm{p0.2},\theta}/\gamma_{\mathrm{M,fi}}$